m^{6}A modification of TERRA RNA is required for telomere maintenance and is a therapeutic target for ALT positive Neuroblastoma

Roshan Vaid[1†], Ketan Thombare[1†], Akram Mendez[1], Rebeca Burgos-Panadero[1], Anna Djos[1], Daniel Jachimowicz[2], Christoph Bartenhagen[3], Navinder Kumar[4], Carina Sihlbom[5], Susanne Fransson[1], John Inge Johnsen[6], Per Kogner[6], Tommy Martinsson[1], Matthias Fischer[3], Tanmoy Mondal[1,7*]

[1]Department of Laboratory Medicine, Institute of Biomedicine, University of Gothenburg, Gothenburg, Sweden.

[2]Translational Genomics, Discovery Biology, Discovery Sciences, BioPharmaceuticals R&D, AstraZeneca, Gothenburg, Sweden.

[3]Department of Experimental Pediatric Oncology, University Children's Hospital of Cologne, Medical Faculty, Cologne, Germany, Center for Molecular Medicine Cologne (CMMC), University of Cologne, Cologne, Germany, Department of Pediatric Oncology and Hematology, University of Cologne, Cologne, Germany.

[4]Department of Microbiology and Immunology, Institute of Biomedicine, University of Gothenburg.

[5]Proteomics Core Facility, Sahlgrenska Academy at the University of Gothenburg, Medicinaregatan 5, 41390 Gothenburg, Sweden.

[6]Childhood Cancer Research Unit, Department of Women's and Children's Health, Karolinska Institute, and Pediatric Oncology, Astrid Lindgren Children's Hospital, Karolinska University Hospital, Stockholm, Sweden.

[7]Department of Clinical Chemistry, Sahlgrenska University Hospital, Gothenburg, Sweden.

[†]**Equal contribution**

[*]Corresponding author, tanmoy.mondal@gu.se.

Department of Clinical Chemistry, Bruna Stråket 16, Sahlgrenska University Hospital, Gothenburg University, Gothenburg, 41345, Sweden.

Abstract:

Telomerase-negative tumors can maintain telomere length by alternative lengthening of telomeres (ALT) but the mechanism behind ALT is poorly understood. Aggressive Neuroblastoma (NB), in particular, relapsed tumors are positive for ALT (ALT+) which suggests that better dissection of the ALT mechanism could provide novel therapeutic opportunities. TERRA long non-coding RNA (lncRNA) which is derived from the telomere ends is localized to telomeres in R-loop dependent manner and is essential for telomere maintenance. In the present study, we provide evidence that RNA modification at the N^6 position of internal adenosine (m^6A) in TERRA RNA by methyltransferase METTL3 is essential for telomere maintenance in ALT+ cells and that loss of TERRA m^6A/METTL3 leads to telomere damage. We observed that R-loop enriched TERRA is abundantly m^6A modified and m^6A mediated recruitment of hnRNPA2B1 to TERRA RNA is essential for R-loop formation. Our data suggest that m^6A drives telomere targeting of TERRA via R-loop and this m^6A mediated R-loop formation could be a widespread mechanism utilized by other chromatin-interacting lncRNAs. Furthermore, treating ALT+ NB cells with METTL3 inhibitor leads to compromised telomere targeting of TERRA and accumulation of DNA damage over telomere, suggesting METTL3 inhibition could be a therapeutic opportunity for ALT+ NB.

Introduction:

RNA modification at the N^6 position of internal adenosine (m^6A) plays a critical role in regulating RNA splicing and many key steps in RNA metabolism. m^6A modification in RNA contributes to a wide range of cellular functions like stress response, DNA damage, cellular differentiation, and the regulation of oncogenes and tumor suppressor gene functions (1). METTL3 is the key enzyme in complex with METTL14 and WTAP, which deposits m^6A in RNA. Active chromatin marks H3K36me3 together with adaptor protein RBM15 and VIRMA (also known as KIAA1429) is thought to guide METTL3 complex to RNA substrates to perform m^6A modification (2-4). The "DRACH" like motif is the most preferred site for m^6A modification however, other non-canonical motifs can also be used for m^6A deposition by METTL3 (5). m^6A modification can also be dynamically regulated as m^6A demethylase like ALKBH5 can remove m^6A from the transcript (6). Once m^6A is deposited in RNA, reader proteins in the nucleus (i.e. YTHDC1, RBMX, hnRNPA2B1) and cytoplasmic (YTHDF1/2/3) identify m^6A residues to guide the functional complex to the modified RNA (1,7,8). Recently it has been shown that chromatin binding of METTL3 and METTL14 in both promoter and distal enhancer elements has been shown to regulate the transcriptional process (9). m^6A

68 modification in retrotransposon-derived transcripts modulates the local chromatin structure to
69 regulate transcription (5,10). RNA strand of the RNA:DNA hybrid containing R-loop structure
70 is enriched with m^6A modification and METTL3 depletion affects the global level of the R-
71 loop (11,12). How m^6A modification in the RNA modulates the R-loop level and the functional
72 significance of the presence of m^6A in the R-loop structure require further investigation.
73 The role of m^6A modification in long non-coding RNA (lncRNA) function is evident in several
74 studies (13,14). The *cis*-acting lncRNA *Xist* which localizes to inactive X-chromosome is m^6A
75 modified at several residues in both the "DRACH" and non- "DRACH" motif context. Xist is
76 associated with adaptor protein RBM15 which recruits the METTL3/METTL14 complex to
77 deposit m^6A on *Xist* RNA. The reader protein YTHDC1 has been shown to recognize m^6A in
78 the UCG tetra-loop of Repeat A in the *Xist* RNA and to be required for *Xist* mediated gene
79 silencing (3,15). The presence of m^6A modification is also detected in non-canonical GGAAU
80 motif in HSATIII lncRNA and has been shown to be critical for the sequestration of splicing
81 factors in nuclear stress bodies (16). Wide-spread m^6A modification is also detected in several
82 chromatin-bound RNAs including enhancer RNAs, and promoter-associated RNAs (17). m^6A
83 modification of enhancer RNAs has been shown to be required for YTHDC1 and BRD4
84 mediated transcriptional activation of neighboring genes (18). But how m^6A modification
85 influences the chromatin localization of lncRNAs to the specific genomic locus is not well
86 understood.
87 TERRA (telomeric repeat-containing RNA) is a lncRNA derived from the subtelomeric ends
88 that contain telomeric repeats in the mature transcript (Feretzaki et al., 2020). TERRA
89 promoters can be located within 1-2 kilobases (kb) from telomere ends to several kb away from
90 the telomere end. TERRA lncRNAs are transcribed by RNA polymerase II (RNA Pol II) that
91 moves towards the telomere ends and thus incorporates UUAGGG containing telomeric repeats
92 (19,20). TERRA RNA is shown to be localized to telomere both in *Cis* and *trans*-acting manner
93 and RAD51/BRCA1 driven R-loop formation is required for this process (21). TERRA
94 transcription is upregulated in tumor cells positive for alternative lengthening of telomeres
95 (ALT+) and is thought to contribute to the maintenance of long telomeres. It is unknown what
96 additional factors are involved in R-loop mediated TERRA targeting in ALT+ cells.
97 Understanding chromatin targeting of TERRA RNA might shed light on the mechanism
98 utilized by other *cis* and *trans*-acting lncRNA for their chromatin recruitment. As R-loop
99 formation can be regulated in m^6A dependent manner, we wanted to explore if m^6A
100 modification has any role in TERRA function. The telomere capping protein TRF2 has also
101 been found to be interacting with the m^6A related proteins (RBM15 and ALKBH5) but the

102 significance of this interaction is unknown (22,23). Recently it has been shown that G-
103 quadruplex derived from TERRA repeats and other G-quadruplex forming sequences has been
104 shown to bind METTL14, but if such sequences have any role to drive m^6A modification in
105 TERRA RNA is not known (24)
106 NB is the most common extracranial solid tumor in children, and it is highly heterogeneous in
107 its clinical and biological nature. The presence of telomere maintenance mechanisms in NB
108 has been proposed to in part explain the heterogeneity of NB tumors and disease outcomes.
109 The presence of telomere maintenance mechanisms are strongly associated with high-risk NB.
110 By contrast, telomere maintenance mechanisms are absent in spontaneously regressing low-
111 risk tumors. In the majority of high-risk cases, telomere maintenance is conferred by
112 telomerase, which is induced transcriptionally, e.g., through the oncogene MYCN, or by
113 genomic translocations leading to enhancer hijacking events (25). In roughly one-third of high-
114 risk NB, however, telomeres are maintained by the alternative lengthening of telomeres (ALT)
115 pathway, which is characterized by long telomeres and ALT-associated promyelocytic
116 leukemia nuclear bodies (APBs) (26,27). The molecular mechanisms underlying ALT are still
117 poorly understood, despite advancements over recent years (28). This suggests a deeper
118 understanding of the biology of ALT+ tumors and systematic investigation of the molecular
119 mechanism of ALT may help us to identify potential therapeutic targets for these clinically
120 unfavorable high-risk NB tumors with the significant need for new better treatment options.
121 In the present study, using well-characterized ALT+ U-2 OS cells we have dissected the role
122 of m^6A RNA modification in the TERRA RNA and characterized the significance of such
123 modification in R-loop formation. We also show that METTL3 mediated m^6A modification of
124 the TERRA is essential for telomere maintenance in ALT+ NB cells and inhibiting METTL3
125 could be a therapeutic option for ALT+ NB tumor
126
127 **Results:**
128 **TERRA RNA is enriched with m^6A modification**
129 To check if TERRA RNA is m^6A modified or not, we have performed m^6A RNA Immuno-
130 precipitation (m^6A RIP) with m^6A antibody in ALT+ U-2 OS cells prior slot blot with a probe
131 against telomeric repeats. Through this we observed the enrichment of TERRA RNA and that
132 m^6A enrichment of TERRA RNA was sensitive to RNase A treatment (**Figure 1A**). To
133 investigate if m^6A modification of is located in telomeric repeats or elsewhere in TERRA
134 transcript, we have performed m^6A RIP with both fragmented and non-fragmented RNA under
135 the assumption that if m^6A modifications are present in telomeric repeat sequences, extensive

136 fragmentation (<150 nt) will have a low impact in TERRA m^6A enrichment when detected
137 with a probe against telomeric repeats in the slot blot assay. On the other hand, if major m^6A
138 modification is located in non-repetitive regions of TERRA RNA, m^6A enrichment will have
139 a more profound effect after fragmentation. As no major difference in TERRA enrichment was
140 seen between fragmented and non-fragmented RNA, this indicated that the major fraction of
141 m^6A modifications in TERRA RNA is located in telomeric repeat sequences (**Figure 1B, C,**
142 **and Supplementary Figure S1A**). TERRA m^6A enrichment was compromised in METTL3-
143 KD cells in both the non-fragmented and fragmented RNA (**Figure 1C**).
144 To confirm the presence of m^6A in TERRA repeats we purified TERRA from total RNA using
145 biotin-labeled probe antisense to TERRA along with negative control (probe against Luciferase
146 RNA) (**Figure 1D**). We verified TERRA enrichment only with the TERRA antisense probe
147 but not with the negative control probe and this enrichment was sensitive to RNase A treatment
148 (**Figure 1E**). Further, purified TERRA RNA along with synthesized RNA oligo standard
149 containing TERRA repeats with or without m^6A modification were digested with ribonuclease
150 T1 (RNase T1) and were subjected to RNA mass spectrometry (RNA-MS) analysis (**Figure**
151 **1D and F**). Using the RNA-MS and higher-energy collisional dissociation (HCD) tandem MS
152 (MS2) data we could confirm the presence of UUAGp and UUm^6AGp fragments in our oligo
153 standards (**Figure 1F**). Utilizing this MS2 information from the standards, we could identify
154 the UUAGp tetramers in the complex mixture of other RNA fragments generated by RNase T1
155 cleavage. HCD MS2 analysis further confirmed m^6A modification in the UUAGp tetramer
156 (UUm^6AGp) and approximately 21% of UUAGp fragments were m^6A modified (**Figure 1F**).
157 To validate further if the telomeric repeat sequence in TERRA could be m^6A modified, we
158 have performed an *in vitro* m^6A methyltransferase assay using a purified METTL3/METTL14
159 enzyme complex. As a substrate, we have used either synthesized TERRA oligo $(UUAGGG)_3$
160 or DRACH oligo $(GGACU)_3$ followed by treatment with Nuclease P1 and liquid
161 chromatography-tandem mass spectrometry (LC-MS/MS)LC/MS analysis to detect A/m^6A
162 (**Supplementary Figure S1B**). Synthesized standard oligo with or without m^6A were digested
163 parallelly with Nuclease P1 and included in the LC-MS/MS. Employing the parallel reaction-
164 monitoring (PRM) mode, we screened LC-MS/MS profiles for A and m^6A which corresponds
165 to m/z 268.0–136.0 and m/z 282.0–150.1 respectively (29) (**Supplementary Figure S1B**). We
166 observed *in vitro* m^6A modification of both TERRA and DRACH oligo by
167 METTL3/METTL14 complex (**Supplementary Figure S1B**). Although the efficiency of m^6A
168 modification in TERRA oligo was less compared to the canonical "DRACH" oligo as detected

169 by the A/m^{6}A ratio (**Supplementary Figure S1B**), nevertheless our data support
170 METTL3/METTL14 complex can modify telomeric repeats in TERRA RNA**.**
171 We checked if METTL3/METT14 complex is localized over the telomeres in ALT+ U-2 OS
172 cells. We performed a proximity ligation assay (PLA) using TRF2 in combination with either
173 METTL3 or METTL14 (**Figure 1G**). We observed an overlap of METTL3/TRF2 and
174 METTL14/TRF2 PLA signal with telomeres detected by TRF1-mCherry. The negative control
175 PLA with a single antibody did not give any TRF1-mCherry overlapping signal (**Figure 1G**
176 **Supplementary Figure S1C**). Using Chromatin Immuno-precipitation (ChIP) we also
177 observed that METTL3 is recruited to telomere chromatin in U-2 OS cells (**Supplementary**
178 **Figure S1D**) suggesting METTL3 is the m^{6}A methyltransferase for TERRA RNA.
179 We performed RNA *in situ* hybridization to validate the TERRA RNA localization at telomeres
180 and we observed TERRA foci frequently overlapped with the TRF1-mCherry signal (**Figure**
181 **1H**). We have also verified the specificity of TERRA RNA foci using locked-nucleic acid
182 (LNA) mediated KD of TERRA RNA (**Supplementary Figure S1E**). Using a modified RNA-
183 situ hybridization protocol which reduces the background in m^{6}A immuno-staining (30) we
184 next checked if TERRA foci overlapped with m^{6}A, and we found a frequent overlap of m^{6}A
185 and TERRA foci further suggesting the presence of m^{6}A modification on TERRA RNA
186 (**Figure 1I**).
187 To explore further TERRA expression and m^{6}A modification we have performed short
188 (Illumina) and long reads (ONT: Oxford Nanopore Technologies) RNA-seq and m^{6}A RIP-seq
189 in Control-sh and METTL3-KD U-2 OS cells (**Figure 2A**). To better map sequencing reads to
190 telomere ends, we utilized the latest Telomere to telomere (T2T) human genome assembly (31)
191 for our RNA-seq data analysis specifically focusing on subtelomeric regions. Combine with
192 strand-specific Illumina short reads and ONT long-reads we could identify transcriptionally
193 active and inactive subtelomeres from both p and q arms of chromosomes (**Figure 2B**). As
194 TERRA RNAs are transcribed in the direction towards the telomere ends, consistent with this
195 strand-specific Illumina short reads were mainly derived from one of the strands depending on
196 from which chromosome arms (p and q) they are originating (**Figure 2B and Supplementary**
197 **Figure 2A**). By remapping available CTCF ChIP-seq data to T2T assembly, we observed both
198 proximal and distal CpG islands located over subtelomere, are flanked by CTCF sites as
199 reported earlier (**Figure 2B**) (32). Using available RNA Pol II ChIP-seq data we also find
200 occupancy of RNA Pol II at actively TERRA transcribing chromosome ends (**Figure 2B**).
201 Considering the repetitive nature of chromosome ends we employed mappability normalization
202 to RNA-seq data. Mappability normalized short and long reads RNA-seq data was used to

define high and low TERRA expressing subtelomeres using the reads covering 30 kb (distance from the last consecutive Telomeric repeats) of subtelomeric regions which include both proximal and distal CpG islands. We observed consistent activity of high TERRA expressing subtelomere in both short and long-read RNA-seq datasets (**Figure 2C, Supplementary Figure S2B and C**). Though METTL3-KD shows a trend of decreased TERRA RNA level compared to Control-sh cells these differences were not statistically significant (**Supplementary Figure S2B and C**). However, we observed a minor (~15%) but significant decrease in TERRA expression in METTL3-KD cells compared to control-sh using the slot blot assay (**Supplementary Figure S2D**).

Once we establish the subtelomeric TERRA expression profile in U-2 OS cells we wanted to check if the telomeric repeats and subtelomeric sequences are enriched with m^6A modifications. We employed a few changes in the m^6A RIP-seq protocol so that we could profile m^6A with less amount of RNA (33) while preserving the strand information of the RNA-seq data. We also used bacterial RNA as a spike-in control in our m^6A RIP-seq protocol which allowed us to accurately normalize the data (**Figure 2A**). The m^6A distribution from RIP-seq performed on U-2 OS nuclear RNA was very similar as described earlier (5), with major m^6A peaks at 3´UTR and enrichment of "DRACH" motif (**Supplementary Figure S2E and F**). In the m^6A RIP-seq data from METTL3-KD cells, we observed an overall decrease in m^6A peaks compared to the control suggesting the specificity of the m^6A RIP-seq (**Supplementary Figure S2G**).

We have quantified the amount of telomeric repeat reads present in m^6A RIP-seq data and we found higher enrichment of telomeric repeat reads in Control-sh compared to METTL3-KD and IgG control (**Supplementary Figure S2H**). Further, we observed that TERRA RNA from several subtelomeric regions is enriched with m^6A modifications (m^6A/input ratio) and this enrichment was affected in METTL3-KD cells (**Figure 2D**). We detected m^6A peaks in the subtelomeres and we see an overall decrease in subtelomere-associated peaks in METTL3-KD cells (**Figure 2C**). To visualize m^6A enrichment across the several active and inactive subtelomere together, we plotted mappability and spike-in normalized m^6A RIP-seq signal over input ($\log_2$ m^6A/input) obtained from Control-sh and METTL3-KD cells over the 30kb subtelomeric regions as metagene plots. We observed m^6A enrichment over subtelomere in Control-sh cell and this was significantly decreased after METTL3-KD (**Figure 2E and F**).

A recent report suggests that "DRACH" like sequences in TERRA can also contribute to m^6A modification (34). We observe the presence of the DRACH sequence in the subtelomeric m^6A peaks and m^6A enrichment ($\log_2$ m^6A/input) over the DRACH sequence was modestly but

237 significantly decreased in METTL3-KD compared to Control-sh (**Supplementary Figure**
238 **S2J**).
239
240 We also used long-read RNA-seq data from Control-sh and METTL3-KD cells to identify
241 differentially modified m^6A sites. Among the 27125 significantly modified NNANN sites
242 identified by xPore (35) genome-wide, 26952 could be successfully translated to annotated
243 gene coordinates. The differentially modified "m^6A" sites follow similar 3´UTR enrichment
244 like m^6A RIP-seq peaks with considerable overlap between the two m^6A detection methods
245 (**Supplementary Figure S2E and I).** We also observed the enrichment of the "DRACH" like
246 motif in the long-read detected m^6A sites as well (**Supplementary Figure 2F**). Next, we refine
247 the search for possible m^6A sites at chromosome ends especially focusing on the non-repeated
248 part of subtelomeres given inherent base calling errors in Nanopore long-read sequencing at
249 telomeric repeats (36). To this end, we performed a transcriptome assembly based on the long-
250 reads mapped to the T2T reference genome and identified 92 NNANN sites that were
251 differentially m^6A modified between Control-sh and METTL3-KD and are located within the
252 last 30 kb regions of subtelomere ends (as defined above) with 6 of them having a DRACH
253 motif (Supplementary **Figure S2K**). Subtelomere with higher TERRA expression also contains
254 more differentially detected m^6A sites in ONT reads compared to low expressed ones and these
255 sites frequently overlap with m^6A RIP-seq detected peaks (**Figure 2C and D**).
256 Collectively, we demonstrate that TERRA RNA undergoes m^6A modification in both telomeric
257 repeats and subtelomeric non-repeated regions which frequently contain a "DRACH" like
258 motif.
259
260 **METTL3 mediated m^6A modification of TERRA RNA is required for telomere**
261 **maintenance in ALT+ cells**
262 We next wanted to explore the importance of m^6A modification on TERRA RNA. As evident
263 from the results above, TERRA RNA forms foci over telomeres in the U-2 OS cells and these
264 foci are sensitive to TERRA KD (**Figure 1H and Supplementary Figure S1E**). We first tested
265 the role of m^6A modification on TERRA RNA foci formation by performing RNA FISH on U-
266 2 OS cells that had transient KD (siRNA) of METTL3. We observed that TERRA RNA foci
267 formation was compromised in the METTL3 siRNA-treated cells compared to control siRNA
268 treatment (**Figure 3A, Supplementary Figure S3A**). As we observed METT3/METTL14 co-
269 localize over ALT telomeres (**Figure 1G**), so we also tested the effect of siRNA mediated
270 depletion of METTL14 on TERRA foci formation. Similar to METTL3, METTL14 depletion

271 by siRNA leads to compromised TERRA foci formation (**Supplementary Figure S3B**). The
272 loss of TERRA RNA foci was further validated in stable KD of METTL3 in the U-2 OS cells
273 (**Figure 3B**). TERRA RNA is thought to contribute to the maintenance of telomeres, therefore
274 we sought to address the significance of TERRA RNA m^6A modification on telomere
275 maintenance. To this end, we performed immuno-fluorescence staining with γ-H2AX, a DNA
276 damage response marker, and TRF2 (to mark the telomere) in control and METTL3-KD cells.
277 We observed that METTL3-KD leads to a higher accumulation of γ-H2AX over telomere
278 compared to control cells, indicating higher telomere damage in cells lacking METTL3 (**Figure**
279 **3C**). Higher γ-H2AX deposition over telomere was also noticed in the TERRA depleted cells
280 as well (**Supplementary Figure S3C**), suggesting TERRA is required for telomere
281 maintenance in ALT telomeres. Consistent with telomere damage in METTL3-KD cells we
282 also observed an increase in TRF2 overlapping Promyelocytic leukemia (PML) bodies
283 (**Supplementary Figure S3D**).
284 Recent publications have elucidated the role of METTL3 mediated m^6A modification in DNA
285 damage response (37,38). We reasoned if we create telomere DNA damage exogenously using
286 bleomycin (a well-characterized DNA damaging agent) in our U-2 OS cells (39), it will allow
287 us to dissect the role of TERRA m^6A modification in such repair processes. We treated control
288 U-2 OS cells with bleomycin and detected DNA damage by the accumulation of γ-H2AX over
289 the telomere within 4 hours of treatment. Interestingly if we allow the U-2 OS cells to recover
290 (20 hours) post bleomycin treatment, γ-H2AX accumulation was significantly reduced over
291 telomere (**Figure 3D**). However, in the METTL3-KD cells, this accumulation of γ-H2AX did
292 not cease, but rather increased, even after cells were off media containing bleomycin for 20
293 hours (**Figure 3D**). We observed a higher number of m^6A overlapping TERRA foci, during
294 recovery post bleomycin treatment in U-2 OS cells suggesting the role of TERRA m^6A in
295 telomere damage repair (**Figure 3E**).
296 To elucidate the importance of m^6A modification on TERRA RNA, we specifically removed
297 m^6A modification from TERRA RNA using RNA-guided CRISPR/dCasRx system (40).
298 Catalytically dead RNA CRISPR/dCasRx fused with m^6A demethylase- FTO (dCasRx-FTO)
299 was recruited to TERRA RNA to specifically remove m^6A from TERRA repeats in U-2 OS
300 cells (41) (**Figure 3F**). We verified the removal of m^6A from TERRA RNA by performing
301 m^6A RIP followed by TERRA slot blot, as evident from the blot, recruiting of dCasRx-FTO to
302 TERRA resulted in a lower enrichment of m^6A over TERRA RNA compared to non-template
303 control (NTC) (**Figure 3G**). Recruitment of dCasRx-FTO by TERRA gRNA did not result in

304 any change in TERRA RNA (**Supplementary Figure S3E**). We next evaluated the effect of
305 this specific removal of m^6A on the ability of TERRA RNA foci formation by performing
306 TERRA RNA-FISH. We observed a loss of TERRA foci in cells where dCasRx-FTO was
307 recruited to TERRA (**Figure 3H**). To test the specificity of guide RNA, instead of recruiting
308 dCasRx-FTO we deployed catalytically active CasRx and checked if TERRA RNA was
309 downregulated. As expected, we saw lower levels of TERRA RNA in cells where CasRX was
310 recruited at TERRA RNA compared to NTC (**Supplementary Figure S3F**).
311 Owing to the growing importance of METTL3 mediated m^6A modification in diseases, in
312 recent years two independent studies developed METTL3 inhibitors (42,43). In particular,
313 Yankova et al. extensively tested a small molecule METTL3 inhibitor in various AML mouse
314 models and concluded that METTL3 inhibition is a potential therapeutic strategy in AML (42).
315 We wanted to test the effect of these available METTL3 inhibitors on TERRA RNA foci
316 formation. Treatment with Actinomycin D (ActD) which blocks RNA Pol II thereby the
317 synthesis of new RNAs, suggests one hour of ActD treatment leads to a major depletion of
318 existing TERRA (**Supplementary Figure S3G**). Keeping the TERRA half-life in
319 consideration obtained from ActD data (**Supplementary Figure 3G**), we treated U-2 OS cells
320 for 6 hours with two METTL3 inhibitors (STM2457 and UZH1A), which will lead to
321 compromised deposition of m^6A in the newly formed TERRA molecules. We observed a
322 pronounced reduction in TERRA RNA foci following 6 hours of METTL3 inhibition compared
323 to DMSO control (**Figure 2I**). Whereas treatment with inefficient METTL3 inhibitor (UZH1B)
324 (43) at the same time had a relatively less pronounced effect on TERRA foci (**Figure 3I**).
325 Treatment with METTL3 inhibitor STM2457 which showed the highest effect on TERRA foci
326 did not alter TERRA RNA level as compared to DMSO control (**Supplementary Figure S3H**).
327 By modulating the m^6A using either the dCasRx-FTO system or by METTL3 inhibitor
328 treatment, we unravel the critical role of m^6A modification in the functionality of TERRA
329 RNA. Our data collectively suggest that METTL3 mediated m^6A modification of TERRA is
330 vital for TERRA RNA foci formation and m^6A modification in TERRA RNA is required for
331 the repair of the damaged telomeres.

332 **hnRNPA2B1 binds TERRA RNA in m^6A dependent manner and is required for TERRA**
333 **function**

334 Our result so far suggests that METTL3 mediated m^6A modification of TERRA RNA is
335 required for TERRA foci formation. Next, we wanted to evaluate if m^6A reader proteins are
336 involved in this process. We performed a small siRNA screen to knock down known m^6A
337 reader proteins such as YTHDC1, hnRNPA2B1, RBMX (Nuclear m^6A readers), and YTHDF2

338 (cytoplasmic reader) (**Figure 4A, Supplementary Figure S4A**). Among these hnRNPA2B1
339 and YTHDC1 have been shown to interact with TERRA RNA before (34,44). We observed
340 that out of all m^6A reader proteins tested hnRNPA2B1 KD had a major effect on TERRA foci
341 formation (**Figure 4A**). Though we observed the loss of TERRA RNA foci in hnRNPA2B1
342 KD cells but TERRA level was unchanged (**Supplementary Figure S4B**). We could also
343 validate hnRNPA2B1 interaction with TERRA RNA using RNA Immunoprecipitation (RIP)
344 followed by slot blot (**Figure 4B**). Next, we asked how a change in TERRA m^6A level
345 contributes to hnRNPA2B1 interaction. To this end, we performed hnRNPA2B1 RIP in
346 Control-sh and METTL3-KD cells followed by TERRA slot blot. We observed reduced
347 hnRNPA2B1 interaction with TERRA in METTL3-KD cells, suggesting a role of m^6A
348 modification in TERRA and hnRNPA2B1 interaction (**Figure 4C**). To check further if
349 hnRNPA2B1 enriched TERRA was m^6A modified or not, we performed m^6A RIP using
350 hnRNPA2B1 bound RNA and observed hnRNPA2B1 interacting TERRA RNA was modified
351 with m^6A (**Figure 4C**). Consistent with our RIP experiment purified hnRNPA2B1 interacts
352 efficiently with TERRA RNA derived from control U-2 OS cells but with reduced efficiency
353 with TERRA derived from METTL3-KD cells (**Supplementary Figure S4C**). Finally, when
354 we specifically demethylate TERRA RNA by deploying dCasRx-FTO, we see reduced
355 occupancy of hnRNPA2B1 at telomere (**Figure 4D**). To know if hnRNPA2B1 KD phenocopy
356 the increased DNA damage phenotype at telomers as observed in METTL3-KD cells, we
357 immuno-stained γ-H2AX and TRF2 in U-2 OS cells following hnRNPA2B1 KD. KD of
358 hnRNPA2B1 resulted in increased accumulation of γ-H2AX at telomeres (**Figure 4E**). Our
359 results demonstrate that the binding of hnRNPA2B1 and m^6A co-operate with each other for
360 TERRA dependent maintenance of telomere in ALT+ cells.
361
362 **TERRA m^6A modification promotes R-loop formation**
363 Recent studies reported that m^6A modification is present in the R-loop and might contribute to
364 R-loop formation (11,12). R-loop formation by TERRA is also critical for targeting TERRA to
365 the telomere (21). We observed lack of m^6A in TERRA RNA leads to a decrease in TERRA
366 RNA foci and this could be attributed to compromised telomere targeting of TERRA RNA.
367 We reasoned that a decrease in TERRA R-loop formation in the absence of m^6A might lead to
368 inefficient targeting of TERRA to the telomere. We modified the published DNA-RNA
369 immunoprecipitation (DRIP) protocol, where anti-RNA:DNA hybrid S9.6 antibody is used to
370 identify RNA strand of R-loops, keeping two goals; (i) to measure accurately TERRA RNA

371 present in the R-loop structures and (ii) to identify if TERRA RNA in R-loop context is m^6A
372 modified. To obtain specific enrichment of R-loop associated TERRA RNA we treated the cell
373 lysate with RNase A briefly to remove free RNA from the subsequent genomic DNA isolation
374 step (**Figure 5A**). We also treated isolated genomic DNA before S9.6 IP with RNase III which
375 is shown to remove non-specific enrichment of double-stranded RNA fragments to identify
376 genuine R-loop enriched RNAs (**Figure 5A**)(45). We pre-treated genomic DNA with RNase
377 H to cross-check the specificity of S9.6 IP as a control (**Figure 5A**). Following S9.6 IP we
378 performed extensive DNase I treatment to obtain R-loop associated RNA (**Figure 5A**). We
379 further used R-loop associated RNA for slot blot assay and we could successfully detect
380 enrichment of R-loop associated TERRA (hereafter referred to as RL-TERRA) (**Figure 5B**).
381 RL-TERRA enrichment was decreased following RNase H treatment, and no enrichment was
382 observed with IgG control (used as negative control) suggesting the specificity of the obtained
383 RL-TERRA using our modified DRIP method. Enriched RL-TERRA was sensitive to RNase
384 A treatment as well (**Figure 5B**). Next, we used R-loop associated RNA obtained from our
385 modified DRIP method (as described above) as input for m^6A RIP, we refer to this complete
386 protocol as DRImR (**DR**IP followed by **m**^{6}A **R**IP) (**Figure 5A and B**). DRImR allows us to
387 detect m^6A modification present in R-loop structures. We observed that m^6A modified TERRA
388 was abundantly present in DRImR enriched RNA and this enrichment was sensitive to RNase
389 H treatment showing RL-TERRA is m^6A modified (**Figure 5B**). Further, METTL3-KD leads
390 to compromise RL-TERRA enrichment in U-2 OS cells suggesting TERRA m^6A contributes
391 to R-loop formation (**Figure 5C**).
392 To check the effect of R-loop removal in TERRA foci formation, we treated U-2 OS cells with
393 either RNase A alone or in combination with RNase H. We observed only RNase A had a
394 moderate effect on TERRA RNA foci in U-2 OS cells but combining RNase A and RNase H
395 led to the disappearance of TERRA foci suggesting the importance of R-loops in TERRA foci
396 formation (**Supplementary Figure S5A**). We reasoned if lack of TERRA m^6A in METTL3-
397 KD cells leads to compromised R-loop thereby disturbing TERRA foci formation, and whether
398 this can be rescued by removing RNase H which will allow R-loop accumulation. We could
399 rescue TERRA foci in METTL3-KD cells by further removing RNase H transiently with
400 siRNA, suggesting the role of m^6A in the R-loop driven TERRA foci formation (**Figure 5D,**
401 **Supplementary Figure S5B**).
402 Next, we went ahead to standardize a robust and fast PLA based method to check telomere R-
403 loop in different experimental conditions where we observed TERRA foci were compromised.
404 We used PLA assay with TRF2 and S9.6 antibodies (R-loop PLA) to determine the presence

405 of R-loop over telomere. Telomeres were marked by TRF1-mCherry to further confirm the
406 presence of R-loop PLA signal over telomere. We used wild-type RNase H (RNase H^{WT}) and
407 catalytically inactive mutant RNase H (RNase H^{Mut}) cells as a control in our experiment. As
408 expected, overexpression of RNase H^{WT} leads to a decrease in overall R-loop content
409 (**Supplementary Figure S5C**). RNase H^{WT} cells also show a decreased number of TERRA
410 RNA foci compared to RNase H^{Mut} (**Supplementary S5D**). We observe an overlap of R-loop
411 PLA signal over telomere in the cell expressing RNase H^{Mut} but this signal was considerably
412 decreased in RNase H^{WT} cells suggesting the specificity of our assay in detecting R-loop over
413 telomere (**Figure 5E**). We also did not detect any telomere overlapping PLA signal in single
414 antibody control of S9.6 and anti-TRF2 antibody (**Supplementary Figure S5E**).
415 We applied R-loop PLA to Control-sh and METTL3-KD cells and observed loss of PLA signal
416 over telomere in METTL3-KD cells and this observation is consistent with data obtained using
417 DRImR (**Figure 5C and F**). Further, the removal of TERRA m^6A using dCasRx-FTO and KD
418 of TERRA m^6A reader protein (hnRNPA2B1) also led to a loss of R-loop PLA signal
419 (**Supplementary S5F, Figure 5G**) suggesting TERRA m^6A and its reader hnRNPA2B1 is
420 required for R-loop formation over telomeres. Overall, we provide evidence that m^6A
421 modification of TERRA RNA is required for TERRA R-loop formation thereby TERRA
422 targeting to the telomere**.**
423
424 **In ALT+ NB cells TERRA RNA is m^6A modified**
425 A significant portion of the NB tumors are ALT+ and the prognosis of these patients is poor
426 and a recent study found that relapsed NB tumors are frequently ALT+ (26,27,46,47). The role
427 of TERRA RNA in ALT+ NB tumors has not been investigated in depth. We aim to
428 characterize if m^6A modification of TERRA plays a critical role in telomere maintenance in
429 ALT+ NB. First, we checked TERRA expression in ALT+ and MYCN amplified (ALT-
430 negative: ALT-) NB cell lines. TERRA expression was higher in ALT+ (CHLA-90 and SK-N-
431 F1) compared to ALT- (SK-N-BE(2) and IMR-32) NB cell lines (**Figure 6A**). ALT positivity
432 of NB cell lines was verified by C-circle assay (**Supplementary Figure S6A**). We performed
433 m^6A RIP in fragmented RNA from ALT+ and ALT- NB cell lines and we observed robust
434 enrichment of TERRA with m^6A antibody in ALT+ cells (**Figure 6B**). We also observe
435 prominent TERRA foci in ALT+ but not in ALT- NB cell lines (**Figure 6C**), probably higher
436 TERRA expression and m^6A enrichment in ALT+ cells contribute to TERRA foci formation.
437 TERRA foci in ALT+ NB cells are sensitive to LNA mediated KD and frequently overlap with
438 m^6A immuno-fluorescence signal in the nucleus (**Supplementary Figure S6B and Figure**

439 **6D**). To characterize TERRA expression and m^6A enrichment in ALT+ (SK-N-F1) and ALT-
440 (SK-N-BE(2)) NB cells we performed RNA-seq and m^6A RIP-seq. We observed TERRA
441 expression was low in ALT- cells compare to ALT+ and this is consistent with slot blot assay
442 (**Figure 6A, Supplementary Figure S6C**). We observed enrichment of the "DRACH" motif
443 in the m^6A peaks from both SK-N-F1 and SK-N-BE(2) m^6A RIP-seq data (**Supplementary**
444 **Figure S6D**). Then we went ahead to check subtelomeric m^6A enrichment in these two cell
445 lines, mappability and spike-in normalized subtelomeric m^6A enrichment ($\log_2$ m^6A/input) was
446 significantly higher in ALT+ SK-N-F1 cells compare to ALT- SK-N-BE(2) cells (**Figure 6E,**
447 **F**).
448
449 To get a better view of TERRA expression in NB tumor samples we have compared TERRA
450 expression in representative ALT+ and ALT- tumors for which we had access to RNA. Two
451 of the NB tumors were previously reported by us as ALT+ (26) and for the rest of the used NB
452 tumors, we verified ALT status by C-circle assay (**Supplementary Figure S6E**). We observed
453 elevated levels of TERRA expression in ALT+ tumors and this is consistent with earlier
454 observation (**Figure 6G**)(47). Next, we wanted to characterize TERRA expression and m^6A
455 positivity using RNA-seq and m^6A RIP-seq in two ALT+ NB tumors (NB1 and NB2) which
456 showed high TERRA expression in slot blot (**Figure 6G**). RNA-seq data from ALT+ NB
457 tumors were used to define high and low TERRA expressing subtelomere in a similar way to
458 U-2 OS cells. We observed consistent transcriptional activity from the subtelomeres in both
459 tumors whereas others are silent or moderately transcribed (**Figure 6H, Supplementary**
460 **Figure S6F**). Overall, actively TERRA transcribing subtelomeres are also similar in both NB
461 tumors and U-2 OS cell lines suggesting the commonality in TERRA transcription (**Figure 6I**
462 **and 2C**). We observed that "DRACH" like motifs are enriched in m^6A peaks obtained from
463 both NB tumors (**Supplementary Figure S6G**). TERRA RNAs from several active
464 subtelomeric regions are enriched with m^6A modifications in NB tumors and frequently contain
465 m^6A peaks as well (**Figure 6I, J**). The number of m^6A peaks in NB1 was more compared to
466 NB2 in subtelomere which could be contributed by tumor-specific variations (**Figure 6I**).
467 Subtelomeric metagene profile of mappability and spike-in normalized m^6A enrichment ($\log_2$
468 m^6A/input) suggests high TERRA expressing subtelomeres were more robustly m^6A modified
469 compared to subtelomeres which were lowly expressed in both the ALT+ NB tumors (**Figure**
470 **6K**).
471 We find higher METTL3, METTL14, and hnRNPA2B1 expression in the NB tumor cohort
472 (n=498) significantly associated with poor event free survival (EFS) (**Figure 6L** and

473 **Supplementary Figure S6H**). In a small cohort (n=21) of ALT+ NB tumors, we observed
474 higher METTL3 and METTL14 expression significantly correlated with worst EFS and for
475 hnRNPA2B1 though higher expression tend to show worst EFS, but it did not reach
476 significance (**Figure 6M** and **Supplementary Figure S6I**). We also observed frequent copy
477 number gain of METTL3, METTL14, and TERRA m^6A reader hnRNPA2B1 in ALT+ tumors
478 compared to MYCN amplified NB tumors (**Figure 6N**) suggesting the vital role of METTL3
479 and other m^6A related genes in NB.
480
481 **m^6A modification in TERRA RNA is critical for telomere maintenance in ALT+ NB cells**
482 To explore the role of METTL3 mediated m^6A modification in ALT+ NB, we depleted
483 METTL3 in ALT+ NB cells. We observed siRNA mediated transient removal of METTL3 in
484 ALT+ CHLA-90 and SK-N-F1 cells led to a reduction in the number of TERRA foci similar
485 to U-2 OS cells (**Figure 7A**). We next wanted to check the effect of stable depletion of
486 METTL3 in SK-N-F1 and CHLA-90 cells, but we failed to generate stable METTL3 depleted
487 cells after several attempts as these cells did not survive suggesting METTL3 was essential for
488 the survival of ALT+ NB cells. So, we went ahead to make doxycycline (Dox) inducible TetO
489 METTL3-KD cells (**Supplementary Figure S7A**), and consistent with the observation
490 following stable METTL3 depletion Dox inducible ALT+ cells show a decrease in cell viability
491 and reduction in colony formation compared to TetO Control cells (**Supplementary Figure**
492 **S7B, Figure 7B**). We observed TERRA foci loss in TetO METTL3-KD SK-N-F1 cells (**Figure**
493 **7C**) but TERRA expression was unchanged as visualized in the slot blot assay
494 (**Supplementary Figure S7C**). Dox-induced METTL3 depletion also induces telomere
495 damage in both SK-N-F1 and CHLA-90 cells with a frequent overlap of γ-H2AX with
496 telomeres (**Figure 7D and Supplementary Figure S7D**). METTL3 depletion also leads to a
497 decrease in C-circle formation in these ALT+ NB cells suggesting compromised ALT activity
498 (**Supplementary Figure 7E**). METTL3 depletion in ALT+ NB cells also leads to a decrease
499 in RL-TERRA enrichment like in U-2 OS cells, suggesting compromised TERRA R-loop
500 formation (**Supplementary Figure S7F**). We xenografted TetO Control and METTL3-KD
501 SK-N-F1 and CHLA-90 cells in immuno-compromised mice and we followed the effect on
502 tumor formation following Dox induction. We observed that METTL3-KD leads to reduced
503 xenografted tumor growth in both ALT+ cell lines with a more drastic effect in SK-N-F1 cells
504 (**Figure 7E and Supplementary Figure S7G**).

505 To test if TERRA foci formation in ALT+ NB cells is hnRNPA2B1 dependent, we have
506 depleted hnRNPA2B1, and this led to the loss of TERRA foci (**Figure 7F, G**). We also
507 observed TERRA foci are co-localized with hnRNPA2B1 in ALT+ NB cells (**Supplementary**
508 **Figure S7H**). Finally, we wanted to explore the therapeutic potential of inhibiting the METTL3
509 enzyme in ALT+ NB cell lines. We observed treatment of ALT+ NB cells with METTL3
510 inhibitors STM2457, and UZH1A for 6 hours led to a dramatic decrease in TERRA foci
511 formation compared to cells treated with UZH1B (less potent inhibitor) and DMSO control
512 (**Figure 7H**). We also observed 48 hours of treatment of STM2457 in ALT+ SK-N-F1 cells
513 leads to damaged telomeres which frequently overlapped with γ-H2AX (**Figure 7I**) but
514 STM2457 treatment did not induce any γ-H2AX accumulation over telomeres in MYCN
515 amplified SK-N-BE(2) cells (**Supplementary Figure S7I**). Treatment with STM2457 results
516 in reduced cell viability in SK-N-F1 and CHLA-90 cells (**Supplementary Figure S7J**).
517 Collectively, our data show that TERRA m^6A and METTL3 play a vital role in telomere
518 maintenance in ALT+ NB, and inhibiting METTL3 could be a potential therapeutic target for
519 ALT+ NB.
520
521 **Discussion:**
522 Our study has identified the role of m^6A RNA modification in the telomere-derived noncoding
523 RNA, TERRA, which has a role in the maintenance of telomeres in ALT+ cells. Our data
524 suggest that the METTL3/14 complex is recruited to telomeres in ALT+ U-2 OS cells. Recently
525 G-quadruplex derived from telomeric repeats has been shown to bind METTL14 (24), so it is
526 tempting to speculate that TERRA G-quadruplex might guide m^6A writer METTL3/14 to the
527 telomeres. Removal of METTL3 leads to a decrease in the m^6A modification in the TERRA
528 transcript and loss of TERRA RNA foci in the ALT+ cells. Modulating the m^6A level by
529 METTL3-KD leads to compromised repair of telomeric DNA which is visualized by increased
530 γ-H2AX accumulation over the telomere. Our data suggest that m^6A containing TERRA foci
531 were required for repairing bleomycin induced telomere damage and also that METTL3-KD
532 cells that lack TERRA m^6A failed to repair damaged telomere. In line with our observation, a
533 recent study also reported the role of TERRA m^6A modification in telomere maintenance in
534 ALT+ cells and METTL3-KD induces telomere shortening as well in ALT+ cells (34). They
535 also reported the presence of m^6A modification in TERRA RNA in the subtelomeric sequences.
536 Consistent with this, our m^6A RIP-seq and m^6A sites identified by xPore from long-read RNA-
537 seq data also show that subtelomere-derived TERRA transcripts are enriched with m^6A. Our

538 study using m^{6}A RIP with fragmented RNA (Figure 1B, C), *in vitro* m^{6}A methyltransferase
539 assay of telomeric repeats (Supplementary Figure S1B) and TERRA RNA-MS analysis (Figure
540 1D-F) hinted presence of m^{6}A modification over UUAGGG telomeric repeats in TERRA RNA.
541 Though the efficiency of m^{6}A deposition by METTL3/METTL14 on the telomeric repeats was
542 comparatively low to DRACH sequence *in vitro* however, presence of multiple copies of
543 telomeric repeats in single TERRA molecule could drive effective m^{6}A modification *in vivo*.
544 This m^{6}A modification of TERRA in the repeats could be further enhanced by G-quadruplex
545 like structures present in TERRA RNA (24). Modulating the m^{6}A specifically in the telomeric
546 repeats using dCasRx-FTO recapitulated METTL3-KD phenotype, further suggests the
547 importance of m^{6}A modification at telomeric repeat sequences in TERRA RNA. TERRA
548 subtelomeric sequences containing "DRACH" motif were differentially enriched in m^{6}A RIP-
549 seq data obtained from Control-sh and METTL3-KD cells. The m^{6}A sites detected by xPore
550 include a "DRACH" motif as well. The long-read RNA-seq data was generated using poly-A
551 selected RNA, so this data will not possibly include any m^{6}A sites present in a non-poly-A
552 fraction of TERRA RNA (48). Our m^{6}A RIP-seq and xPore data are consistent with the notion
553 as reported by Chen et al (34) that "DRACH" like sequences in TERRA could also be targeted
554 by METTL3 for m^{6}A modification. Taking together, we provide evidence that both telomeric
555 repeats and subtelomeric sequences contribute to the m^{6}A enrichment of TERRA RNA. Owing
556 to the complexity, that TERRA RNAs are derived from multiple chromosome ends and the
557 presence of telomeric repeats not only at the end of the chromosome but also interspersed in
558 the subtelomeric region (**Figure 2B**), it is challenging to precisely resolve the exact location of
559 m^{6}A modification in the TERRA RNA.
560 Our mechanistic study revealed that m^{6}A modification in TERRA promotes the association of
561 m^{6}A reader hnRNPA2B1. Recently another m^{6}A reader protein YTHDC1 was also shown to
562 interact with TERRA RNA in m^{6}A dependent manner to regulate TERRA RNA stability (34).
563 Though we observed a moderate decrease in TERRA RNA in METTL3-KD U-2 OS cells in
564 the slot blot assay, however, hnRNPA2B1 KD did not alter the TERRA level. TERRA specific
565 m^{6}A removal by an inducible dCasRx-FTO system in U-2 OS cells did not have any impact on
566 steady state level of TERRA RNA. Similarly, we saw unaltered TERRA level in inducible KD
567 of METTL3 in SK-N-F1 cells suggesting that lack of m^{6}A in TERRA might promote TERRA
568 degradation in cell type specific manner or depending on mode m^{6}A of depletion from TERRA
569 RNA. Short term treatment (6 hours) with the METTL3 inhibitor was sufficient to induce loss
570 of TERRA RNA foci without any change in TERRA RNA level, suggesting that m^{6}A
571 modification has a major role in driving telomere targeting of TERRA. But long-term depletion

572 of METTL3 leads to a lack of persistent TERRA targeting to telomeres and this might promote
573 degradation of TERRA RNA, where YTHDC1 mediated stabilization is impaired in the
574 absence of m^6A. Nevertheless, both hnRNPA2B1 and YTHDC1 KD induce telomere damage
575 in ALT+ cells suggesting an important role of the m^6A reader proteins in telomere maintenance
576 (34).
577 The m^6A reader protein hnRNPA2B1 does not have the YTH domain to identify m^6A and has
578 instead been proposed to identify RNA by a "m^6A switch" mechanism (49). It is interesting to
579 note that the motif which is recognized by hnRNPA2B1 is UAGG like sequences (50) whereas
580 the major motif for m^6A is "DRACH" like sequences (51). UUAGGG containing TERRA
581 repeats has been shown to bind hnRNPA2B1 *in vitro* and hnRNPA2B1 also recognise UAGGG
582 containing motifs *in vivo* (52,53). Our *in vitro* and *in vivo* observations suggest m^6A
583 modification in TERRA RNA is critical for hnRNPA2B1 association. We identified the
584 presence of m^6A in the non-canonical UUAGGG context in TERRA. The presence of m^6A in
585 a non-canonical context has also been observed in other lncRNAs such as in HSATIII (AAUG
586 repeats) and Xist (AUCG context in tetra loop of Repeat-A) lncRNAs (15,16). In case of Xist,
587 m^6A sites in AUCG context in Repeat-A create local unfolding which favors YTHDC1
588 recognition (15). "M^6A switch" mechanism also suggests the presence of m^6A creates local
589 folding in RNA thereby enhancing the association of RNA-binding proteins like hnRNPC and
590 RBMX to RNA molecules (8,54).
591 We observed both m^6A modification and hnRNPA2B1 interaction are required for TERRA
592 targeting to telomere by R-loop formation. R-loop associated TERRA (RL-TERRA) was found
593 to be abundantly m^6A modified as detected by DRImR which allows combined detection of
594 RNA strand of R-loop and m^6A modification. It is tempting to speculate that m^6A modification
595 in UUAGGG containing telomeric repeats might promote local unfolding of TERRA RNA
596 during transcription, resulting in efficient recruitment of hnRNPA2B1 and further other repair
597 proteins like RAD51 to promote R-loop formation. R-loop formation is essential for telomere
598 targeting of TERRA after transcription. (21). Chen et al reported compromised RAD51
599 recruitment to telomeres in METTL3-KD cells and defective RAD51 recruitment might affect
600 TERRA dependent R-loop formation (21,34). The mode of chromatin targeting of lncRNAs is
601 still a less understood phenomenon. Increasing evidence suggests that m^6A modification in
602 lncRNAs might promote chromatin association and m^6A modified nascent RNAs accumulate
603 at the site of transcription (55). Our observation from TERRA RNA provides evidence that
604 m^6A mediated R-loop formation might be a general mechanism utilized by other lncRNAs for
605 chromatin targeting (55). Compromise telomere targeting of TERRA in the absence of m^6A

606 might affect the recruitment of DNA repair proteins like BRCA2 which help in recombination-
607 dependent telomere maintenance in ALT+ cells (21). TERRA has also been shown to
608 frequently interact with epigenetic modifiers which are required for telomere maintenance
609 (44,56). In METTL3-KD cells, lack of telomere targeting in TERRA RNA might results in the
610 altered chromatin structure of ALT+ telomeres thereby resulting in a defect in telomere
611 maintenance as well. But the extent of chromatin changes over telomere in METTL3
612 depleted/inhibited ALT+ cells require further study.
613 We observed that ALT+ NB cells are vulnerable to METTL3-KD or METTL3 inhibition.
614 METTL3-KD or inhibition results in the accumulation of telomere damage suggesting
615 METTL3 mediated m^6A modification of TERRA has a very critical role in Telomere
616 maintenance in ALT+ NB cells. TERRA is upregulated in ALT+ NB tumors and ALT+ tumors
617 frequently show a mutation in chromatin remodeler protein ATRX (47). It will be interesting
618 to check if the loss of ATRX has any role in driving TERRA expression and m^6A modifications
619 in ALT+ NB tumors. ALT+ NB tumors show protracted disease phenotype with frequent
620 relapse (47) and higher METTL3 expression correlates with poor disease prognosis in ALT+
621 NB. Our data on METTL3 inhibitor treatment and telomere damage in ALT+ NB cells suggest
622 inhibiting METTL3 could be a novel therapeutic approach for the unfavorable high-risk subset
623 of ALT+ NB tumors.
624
625 **Materials and methods:**
626 **Cell culture**
627 U-2 OS (Sigma-Aldrich) cells were cultured in Dulbecco's modified Eagle's medium (DMEM)
628 supplemented with 10% FBS and penicillin/streptomycin. ALT+ NB cell lines CHLA-90
629 (CCOG) and SK-N-F1 (Sigma-Aldrich) cells were cultured in DMEM media supplemented
630 with 20% and 10% FBS respectively along with penicillin/streptomycin. SK-N-BE(2) cells
631 were cultured in DMEM/F-12 media supplemented with 10% FBS, 4 mM L-glutamine, and
632 penicillin/streptomycin. Cells used in the study were mycoplasma negative and tested
633 routinely.
634 **Plasmids, siRNAs, and molecular cloning:**
635 METTL3 (sh1 and sh2) and Control shRNAs in pLKO.1-TRC cloning vector were purchased
636 from Sigma-Aldrich to generate stable METTL3-KD cells. shRNA sequences are provided in
637 Supplementary Table 1. To generate Dox induced METTL3-KD cells in ALT+ NB METTL3-
638 sh1 sequences were cloned in the Tet-pLKO-puro vector (21915, Addgene). As a control for
639 inducible shRNA KD, we used pLKO-Tet-On-shRNA-Control plasmid (98398, Addgene).

640 dCasRx-FTO-HA plasmid was received as a generous gift from Dr. Wenbo Li´s laboratory
641 (University of Texas Health Science Center, Houston, USA) and CasRx (138149) was obtained
642 from Addgene. The TERRA and negative control gRNAs were cloned in
643 pLentiRNAGuide_002 (138151, Addgene). Sequences of guide RNAs are provided in
644 Supplementary Table 1. RNase H WT and mutant overexpressing vectors were purchased from
645 Addgene (111906 and 111905). TRF1-mCherry plasmid was received as a generous gift from
646 Dr. Emilio Cusanelli (University of Trento, Italy). Pre-designed siRNAs were purchased from
647 either Sigma-Aldrich or Thermo Fisher Scientific and details are provided in Supplementary
648 Table 1. Lentiviral packaging plasmids psPAX2 (12260) and pMD2.G (12259) were obtained
649 from Addgene.

650 ***Gene silencing and overexpression:***

651 Lentiviral based vectors were packaged following instructions from Addgene using packaging
652 plasmids as described above. To generate stable cells antibiotic selection was performed
653 depending on the type of vector used following lentiviral transduction. To generate METTL3-
654 KD cells U-2 OS and ALT+ NB cell lines were selected with media containing Puromycin (1
655 µg/ml). In NB cells Doxycycline (200 ng/ml) was used to induce METTL3-KD. To generate
656 CasRx/dCasRx-FTO and gRNA expressing U-2 OS cells, dCasRx-FTO_HA containing
657 lentivirus were transduced followed by selection with Puromycin (1 µg/ml). The puromycin
658 selected cells were further transduced with gRNA lentivirus and selected with Blasticidin (5
659 µg/ml). To induce CasRx/dCasRx-FTO expression cells were cultured in Doxycycline (200
660 ng/ml) containing media. To generate stable RNase H WT/Mut cell lines corresponding
661 plasmids were transfected using Lipofectamine 3000 reagent (Thermo Fisher Scientific)
662 following manufacturer instruction followed by selection with media containing Hygromycin
663 (400 µg/ml). siRNAs were transfected to induce transient in both U-2 OS and ALT+ NB cells
664 using RNAiMAX (Thermo Fisher Scientific) reagents following the manufacturer's
665 instructions.

666 ***RNA and DNA isolation***

667 *From Cell-lines*

668 RNA was isolated from the cell line using TRIzol reagent (15596026, Thermo Fisher
669 Scientific) and Direct-zol RNA Miniprep (R2050, ZYMO research) or using ReliaPrepTM
670 RNA Cell Miniprep system (Z6011, Promega), according to the manufacturer's instruction.
671 The DNase I treatment step was performed mandatorily, and the RNA was eluted in
672 RNase/DNase-free water.

673 DNA was isolated from cells using the Wizard Genomic DNA purification Kit (Promega)
674 according to the manufacturer's instructions.
675 *From Tumor material*
676 Tumor tissue was collected after written or verbal informed consent was obtained from
677 parents/guardians according to ethical permits approved by the local ethics committees
678 (Karolinska Institute and Karolinska University Hospital Research Ethics Committee,
679 registration number 2009/1369-31/1 and 03-736). RNA was extracted from frozen tumor
680 samples using AllPrep DNA/RNA/Protein Mini Kit (Qiagen) according to the manufacturer's
681 instructions.
682 Genomic DNA was extracted from fresh/frozen tumors or blood using the DNeasy Blood &
683 Tissue kit (Qiagen, Hilden, Germany) according to the manufacturer's instructions. This study
684 was conducted per the Declaration of Helsinki.
685 ***cDNA synthesis and Quantitative PCR (qPCR***
686 RNA was converted to cDNA using the High-Capacity RNA-to-cDNATM Kit (4387406,
687 Thermo Fisher Scientific). qPCR was performed with diluted cDNA (10-fold dilution) as a
688 template and gene-specific PCR primers (Supplementary Table S1) mixed with Power SYBR
689 Green Master Mix (4367659, Thermo Fisher Scientific) using a Quant Studio 3 thermocycler
690 (Thermo Fisher Scientific). The Expression values presented for each gene are normalized to
691 GAPDH using the delta-delta Ct method.
692 ***Slot blot assay***
693 Nucleic acids (RNA or DNA) samples were loaded in Bio-Dot SF Microfiltration Apparatus
694 (Bio-Rad) and allowed to bind onto the membrane. Nucleic acids were UV-crosslinked to the
695 membrane and incubated with prehybridization buffer DIG Easy Hyb (11603558001, Roche,)
696 in a hybridization tube at 37° C for 30 min with rotation. Prehybridization buffer was replaced
697 by hybridization buffer (prehybridization buffer containing 20-50 nM 5′-$(TAACCC)_5$ DIG-
698 labeled probe) and the membrane was hybridized at 37°C overnight with rotation. After
699 hybridization, the membrane was washed with 2x SSC containing 01% SDS for 4x10 min at
700 37°C and equilibrated with washing buffer (0.1 M Maleic acid, 0.15 M NaCl, pH 7.5, 0.3%
701 Tween 20) for 2 min at RT. Next, the membrane was incubated in a blocking buffer (1% (w /
702 v) Roche Blocking Reagent, 0.1 M Maleic Acid, 0.15 M NaCl, pH 7.5) for 30 min at RT.
703 Blocking buffer was replaced with antibody solution (1: 20,000 dilution of Anti-DIG antibody
704 conjugated with alkaline phosphatase in blocking buffer) for 30 min at RT. The membrane was
705 washed twice 2x15 min with washing buffer. The membrane was equilibrated in a detection
706 buffer (0.1 M Tris-HCl, 0.1 M NaCl, pH 9.5) and incubated with CDP-Star Chemiluminescent

707 Substrate (Sigma-Aldrich) inside a hybridization bag. ChemiDoc XRS+ system (Bio-Rad) and
708 ImageLab software were used to detect the signal and quantify the bands.

709 ***TERRA RNA levels using slot blot assay***

710 To check the level of TERRA RNA in different cell lines, tumors, and conditions, isolated total
711 RNA from different samples were first quantified on NanoDrop™ 2000 Spectrophotometer
712 (Thermo Fisher Scientific) and diluted to 30 ng/ul concentration. The diluted RNA was again
713 quantified on the Nanodrop to verify the concentration. The diluted RNA was then loaded onto
714 slot blot in amounts as mentioned in the Figures, and 1 µl of the diluted RNA which
715 corresponds to 30 ng was used as a loading control. The slot blots were probed with a TERRA
716 probe, developed as mentioned above, and normalized to the 28s rRNA signal from the loading
717 control. To obtain the 28s rRNA signal the RNA samples were subjected to electrophoresis on
718 a chip (ScreenTapes) using TapeStation 4200 (Agilent) according to manufactures instruction.

719 ***m^6A RIP followed by sequencing (m^6A* RIP-seq*)/ slot blot***

720 m^6A RIP was performed on RNA as previously described by (33). In brief, for the m^6A RIP-
721 seq experiments the cellular (15 µg/IP) and tumor RNA (4-5 µg/IP) were supplemented with
722 10 ng or 3 ng of bacterial RNA respectively as a spike-in control. For m^6A RIP followed by
723 slot blot bacterial spike-in RNA was not added. The RNA was then subjected to fragmentation
724 using RNA Fragmentation Reagents (AM8740, Thermo Fisher Scientific). m^6A RIP was also
725 performed in one instance without the fragmentation step. RNA immunoprecipitation (RIP)
726 was performed using antibodies against m^6A modification (202003, Synaptic systems) or IgG
727 (sc-2027, Santa Cruz) in RIP buffer (150 mM NaCl, 10 mM Tris-HCl pH 7.5, 0.1% IGEPAL
728 CA-630 and supplemented with RNase inhibitor just before use) for 4 h at 4°C. IgG antibodies
729 served as a negative control for the immunoprecipitation experiments. The immunoprecipitated
730 RNA-antibody complex was captured by incubating with protein A and G magnetic beads
731 (10002D, 10004D, Thermo Fisher Scientific) which were washed twice in RIP buffer. After 2
732 h incubation, the magnetic beads were washed thrice with RIP buffer for 10 min.
733 Immunoprecipitated RNA was eluted either by competitive elution (for RIP-seq) as previously
734 described (33) or by direct extraction using TRIzol (for slot blot).

735 For the m^6A RIP slot blot, the input RNA and the immunoprecipitated RNA were directly
736 subjected to the slot blot assay described above.

737 For m^6A RIP and RNA-seq, sequencing libraries for total RNA-seq/input for m^6A RIP-seq
738 were prepared from 10 ng of the fragmented RNA parallelly along with m^6A RIP samples using
739 SMARTer Stranded Total RNA-seq Kit V2, Pico Input Mammalian (Takara Bio) according to

740 manufactures instructions. All the libraries were single-end sequenced (1x 88 bp) on an
741 Illumina NextSeq 2000 platform at the BEA core facility, in Stockholm, Sweden.

742 ***Processing of m^{6}A RIP-seq data***

743 Raw Illumina short-reads data obtained from SMARTER-Stranded Total RNA-Seq Kit v2
744 sequencing was processed using Trim Galore v0.6.6
745 (https://www.bioinformatics.babraham.ac.uk/projects/trim_galore/) with a minimum length
746 threshold of 20bp. Quality control of Illumina short-reads was performed using FastQC v0.11.9
747 (https://www.bioinformatics.babraham.ac.uk/projects/fastqc/) with default parameters (-q 20).
748 Trimmed reads were mapped with HISAT2 v2.2.1 (57) preserving strand information (-U –
749 rna-strandness R) using the Telomere-to-Telomere (T2T) human reference genome assembly
750 (T2T-CHM13 v1.1) (31). The Escherichia coli K12 genome was concatenated to the T2T
751 reference assembly for further spike-in normalization. To control the systematic variation
752 across m^{6}A RIP experiments, the amount of spiked-in bacterial RNA was estimated by
753 counting the total number of reads uniquely mapping to the E. coli K-12 reference genome
754 using Sambamba v0.7.1 (58). The E. coli spike-in bacterial counts were further used to
755 calculate scaling factors for each batch of m^{6}A RIP-seq samples. Duplicate reads were labeled
756 using MarkDuplicates from Picard v2.23.4 (http://broadinstitute.github.io/picard/). Alignments
757 were downsampled according to calculated spike-in scaling factors using DownsampleSam
758 from Picard (--strategy HighAccuracy). Mapping files were separated by strand after duplicate
759 removal using Sambamba v0.7.1.

760

761 ***Analysis of m^{6}A RIP-seq and ChIP-seq data***

762 Peak calling was performed using MACS v2.2.6 (https://github.com/macs3-project/MACS) on
763 m^{6}A RIP and input alignments normalized to spike-in content, with parameters --no-model, --
764 kee*p*-dup auto, --call-summits, –extsize 75, q-value cutoff of 0.05 and effective genome size
765 according to the T2T-CHM13 v1.1 UCSC table browser. Motif analysis on m^{6}A peaks was
766 carried out using findMotifsGenome.pl from HOMER v4.11 (59). m^{6}A RIP coverage tracks
767 were generated using bamCoverage from deepTools v3.3.2 (60).
768 Public CTCF and RNA Pol II data reported by Deng et al. 2012 (32) were obtained from GEO
769 (GSE1962, GSE19484). Visualization of m^{6}A RIP coverage tracks data was done in R using
770 the rtracklayer (61) and ggplot2 packages (https://www.R-project.org). Telomere coordinates,
771 GC% content, and CpG island coordinates were retrieved from the T2T CHM13 v1.1 reference
772 genome hub (http://t2t.gi.ucsc.edu/chm13/hub/t2t-chm13-v1.1). Telomeric repeat tracks were

773 generated using scanMotifGenomeWide.pl from HOMER v4.11 and bedToBigBed v2.8 from
774 UCSC utilities (62).

775 ***Direct RNA sequencing using Oxford Nanopore Technologies (ONT) long-read***
776 ***sequencing***

777 Total RNA isolated from Control-sh and METTL3-KD cells, 20-25 µg was directly sequenced
778 on the Oxford nanopore platform. In brief Total RNA quantification and quality control were
779 performed on Fragment Analyzer 5300 system and showed RNA integrity number (RIN) of 10
780 for both samples. Poly(A) RNA Selection Kit V1.5 (Lexogen) was used to enrich
781 polyadenylated transcripts with minor changes to the protocol. All the processing volumes were
782 doubled, and 4 µg of Control-sh or METTL3-KD RNA was used as an input in a single
783 reaction. Each sample was batch-processed in 5 separate reactions that were combined at the
784 final elution step. Control-sh and METTL3-KD poly(A)-enriched RNA was analyzed on
785 Fragment Analyzer showing remaining rRNA contamination to be 11% and 21% of mass for
786 each sample respectively. Enriched poly(A)-RNA was then purified using 1x of RNAClean XP
787 (Beckman Coulter) beads to concentrate the sample and remove very short RNA fragments and
788 eluted into 11ul of water. Qubit™ RNA High Sensitivity kit (Invitrogen) was used to quantify
789 the RNA before direct RNA sequencing. SQK-RNA002 (ONT) kit was used for library
790 preparation and followed according to the manufacturer's protocol. Briefly, 400 ng of poly(A)-
791 enriched RNA was used as an input, and recommended reverse-transcription step was
792 performed. Control-sh and METTL3-KD libraries were loaded on individual FLO-MIN106
793 (ONT) flowcells and sequenced on GridION Mk1 device (ONT) for 72 h yielding 1.65 and
794 1.35 million long-reads respectively.

795 ***Processing of direct-RNA Nanopore sequencing data***

796 Direct RNA Oxford Nanopore Technology (ONT) sequencing data was base-called using
797 Guppy v5.0.16 (flowcell FLO-MIN106, kit SQK-RNA002). Quality control was performed
798 with PycoQC (https://github.com/a-slide/pycoQC) and NanoPlot
799 (https://github.com/wdecoster/NanoPlot) on base-called data. ONT reads were mapped to the
800 T2T-CHM13 v1.1 reference genome using the latest version of Minimap (v2.24) (-ma*p*-ont -
801 uf -k14) optimized for mapping long reads to highly repetitive regions (63,64).

802 ***Analysis of ONT data***

803 Identification of m^6A modifications from direct RNA ONT data was performed following the
804 xPore pipeline (https://xpore.readthedocs.io/)(35). xPore allows the identification of m^6A
805 under multiple conditions without the need for unmodified control samples, enabling the
806 quantitative estimation of modification rates from Nanopore sequencing data. Briefly, raw

807 Nanopore signal-level events were aligned to the T2T CHM13 v1.1 reference transcriptome
808 using Nanopolish eventalign v0.12.0. Processed ONT data was further analyzed with xPore
809 (default parameters; minimum read count 5, pre-filtering t-test method, 500 maximum
810 iterations) to estimate the genome-wide RNA modification rates for each independent sample
811 and the differentially modified sites between control and METTL3-KD conditions. A
812 transcriptome assembly was performed using StringTie2 (65) on Nanopore reads, and
813 remapped reads were used with xPore to refine the search for m^6A modifications at
814 chromosome ends. Predicted m^6A sites were selected from differentially modified positions
815 with a base A within the NNANN context with a significance p-value < 0.05 and a differential
816 modification rate (DMR) above zero.

817 **Metagene analysis**

818 Genome-wide distribution of m^6A sites from Illumina and ONT data was analyzed using the
819 plyranges package(66) to map the m^6A coordinates to the genomic feature coordinates (5'
820 UTR, CDS, 3'UTR) obtained from the T2T-CHM13 v1.1 GTF annotation files. Mapped
821 coordinates were further translated to their relative metagene positions. The peak density
822 distribution for all m^6A sites along metagene coordinates was calculated using the density
823 function in R.

824 **Mappability at chromosome ends**

825 To account for the repetitive nature of chromosome ends, we calculated the mappability of
826 short and long reads using GenMap(67). This tool estimates the occurrence of k-mer sequences
827 of a given length across the genome and computes a probability score proportional to its
828 occurrence at different parts of the genome. A mappability score of 1 indicates that a sequence
829 could align to a unique genomic location, while a low mappability value indicates that a
830 sequence can map to one or many sites in the genome. The computed mappability scores for
831 Illumina (75 bp) and Nanopore (600 bp) reads were averaged over fixed-size windows using
832 BEDTools v2.30.0 (68) and further used to normalize the number of reads aligned at each
833 chromosome end to the likelihood of mapping at one or multiple locations.

834 ***Analysis of TERRA expression***

835 To analyze the expression towards chromosome ends in a strand-specific manner, the reads
836 from Illumina alignments mapping to subtelomeric 30 kb regions from chromosome q and p
837 arms were split by strand and filtered from all T2T alignments after duplicate removal.
838 Alignments from direct RNA ONT data were filtered using positive strand information. The
839 number of reads mapping to subtelomeric regions on each chromosome was quantified using
840 the multicov function from BEDTools v2.30.0(68). Expression values were further converted

841 to counts per million (CPM) to normalize for differences in library sizes across samples and
842 normalized to the mappability scores computed using GenMap to adjust for the likelihood of
843 short and long reads to align at one or multiple repetitive sites at each chromosome end.
844 Chromosome ends were classified into two categories (active/inactive) according to their
845 relative CPM expression values, being classified as 'active' if their expression was greater than
846 the median normalized expression value across all chromosomes ends at the control condition
847 and 'inactive' otherwise. Enrichment of telomeric repeats in m^6A RIP-seq from Control-sh,
848 METTL3-KD, and IgG data was calculated using TelomereHunter v1.0.4 using a default repeat
849 threshold of at least 10 non-consecutive repeats to search for TTAGGG, TGAGGG, TCAGGG
850 and TTGGGG repeats (69). Filtered TelomereHunter read counts were normalized using CPM
851 values.

852 ***Immunofluorescence and Proximity ligation assay (PLA)***

853 U-2 OS and NB cell lines (CHLA-90 and SK-N-FI) were seeded on a coverslip in a 24-well
854 plate at a density of 100,000 and 200,000 respectively. In case of NB cells, coverslips
855 (MENZCB00120RAC20, Epredia) were coated with 50 µg/ml collagen (5005, PureCol, Type
856 I Collagen Solution) at RT for 1 h. Cells were fixed using 4% formaldehyde for 10 min
857 followed by 2x washes with PBS and stored in PBS at 4°C until further use.
858 Immunofluorescence was performed using a general protocol. Briefly, cells were
859 permeabilized for 10 min with 0.25% Triton X-100 followed by 3x washes with PBS-T. Cells
860 were blocked with 3% BSA in PBS-T for 30 min and left with primary antibody overnight at
861 4°C. Immunofluorescence was continued the next day starting with 3X PBS-T washes followed
862 by incubation with respective secondary antibodies for 1 h at RT, and then 3X PBS-T washes.
863 Coverslips were dried and mounted on a slide using ProLong Gold Antifade Mountant with
864 DAPI (P36931, Thermo Fisher Scientific). Images were taken using EVOS M7000 microscope
865 (Thermo Fisher Scientific). Information on the used antibodies is provided in Supplementary
866 Table 1.

867 For PLA cell fixation and permeabilization are the same as above. PLA was performed using
868 a Duolink® PLA kit (DUO92014, Sigma-Aldrich) according to the manufacturer's protocol.
869 As a background control single antibody was used in this assay. For R-loop PLA with S9.6 and
870 TRF2 antibodies, cells were pre-treated with RNase A after permeabilization for 30 min at
871 37°C to reduce the backgrounds. Information on the used antibodies is provided in
872 Supplementary Table 1. Images were taken using EVOS M7000 microscope (Thermo Fisher
873 Scientific).

874 ***RNA-FISH***

875 U-2 OS and NB cell lines were seeded on a coverslip in a 24-well plate at a density of 100,000
876 and 200,000 respectively. In case of NB cells, coverslips (MENZCB00120RAC20, Epredia)
877 were coated with 50 µg/ml collagen (5005, PureCol, Type I Collagen Solution) at RT for 1 h.
878 Cells were fixed using 4% formaldehyde for 10 min followed by 2x washes with PBS and
879 stored in 70% ethanol at 4°C until further use. RNA- FISH was performed to detect TERRA
880 RNA and Stellaris RNA FISH protocol for adherent cells was used with some modifications.
881 Briefly, cells were permeabilized for 10 min with 0.25% Triton X-100 followed by a wash with
882 PBS. Cells were then incubated for 2-5 min with wash buffer A (Stellaris RNA FISH Wash
883 Buffer A, SMF- WA1-60, Biosearch Technologies). Hybridization was carried out at 37°C for
884 4 h by incubating cells with hybridization buffer (Stellaris RNA FISH Hybridization Buffer,
885 SMF-HB1-10, Biosearch Technologies) containing TERRA probe $(TAACCC)_7$-Atto488 in a
886 humidified dark chamber. Cells were then washed 2x with wash buffer A at 37°C for 15 min,
887 followed by 2-3 min incubation at RT with wash buffer B (Stellaris RNA FISH Wash Buffer
888 B, SMF- WB1-20, Biosearch Technologies). Coverslips were dried and mounted on a slide
889 using ProLong Gold Antifade Mountant with DAPI (P36931, Thermo Fisher Scientific).
890 Images were taken using EVOS M7000 microscope (Thermo Fisher Scientific).

891 ***Sequential RNA-FISH and immunofluorescence (IF)***

892 For sequential IF staining followed by RNA-FISH as described above cells were fixed using
893 4% formaldehyde for 10 min followed by 2x washes with PBS and stored in 70% ethanol at
894 4°C until further use. Coverslips were rinsed with PBS and cells were permeabilized for 10
895 min using 0.25% Triton X-100 in 1x PBS at RT. Cells were then washed using PBS-T (0.1%
896 Tween-20 in 1x PBS) and blocked in 3% BSA in PBS-T for 30 min. Primary antibodies were
897 diluted in 3% BSA in PBS-T and incubated for 2 h after blocking. 3x5 min washes were
898 performed using PBS-T and incubated for 1 h with secondary antibodies diluted in 3% BSA in
899 PBS-T. 3x5 min washes were performed using PBS-T followed by 10 min fixation by 4%
900 formaldehyde. Cells were rinsed with PBS twice, permeabilized with 0.25% Triton X-100 in
901 1x PBS for 5 min followed by a wash with PBS. TERRA RNA-FISH was performed as
902 described above and proceeded for imaging. Details of antibodies are provided in
903 Supplementary Table 1.

904 ***Simultaneous RNA-FISH and m^6A IF staining***

905 Simultaneous TERRA FISH and m^6A IF were performed as described before (30) with the
906 following modifications. Cells were fixed in MeOH at -20°C for 15 min and TERRA RNA
907 FISH was performed as described above with some modification. After hybridization, during

908 2x30 min washing steps, cold wash buffer A (described above) was added to coverslips and
909 incubated at 37°C. This step allows refolding of rRNAs to reduce the nuclear RNA signal
910 coming from rRNAs as described by Fu et al (30). Coverslips were then washed with wash
911 buffer B (described above) for 2-3 min and then rinsed with 1x PBS. Coverslips were incubated
912 in wash buffer A containing 10% formamide for 5-10 min and followed by blocking for 1 h
913 (3% BSA in PBS-T) and the primary antibody against m^6A was incubated for 2 h at RT in 3%
914 BSA in PBS-T. 3x5 min PBS-T washes were done and the secondary antibody was incubated
915 for 1 h at RT. Coverslips were washed 3x5 min with PBS-T and mounted. Imaging was done
916 using EVOS M7000 microscope.

917 ***Western blot***

918 Cell lysates were prepared using RIPA buffer (R0278, Sigma-Aldrich,) and total protein
919 content was quantified using Pierce BCA Protein Assay Kit (23225, Thermo Fisher Scientific)
920 as per manufacturer's instructions. Equal amounts and volume of samples were resolved by
921 SDS- PAGE on NuPAGE Bis-Tri Gels (4-12%) (Thermo Fisher Scientific), followed by
922 transfer onto 0.2 µm Nitrocellulose membrane using Trans-Blot Turbo Transfer System (Bio-
923 Rad). The membrane was blocked for 1 h at RT with a 5% blocking solution of non-fat dried
924 milk in PBS-T.

925 The membrane was incubated with the primary antibody in a 5% blocking solution overnight
926 at 4°C. Immunoblotting was continued the next day starting with 3x PBS-T washes followed
927 by incubation with respective secondary antibodies for 1 h at RT, and then 3X PBS-T washes.
928 Proteins were detected with SuperSignal West Pico PLUS Chemiluminescent Substrate
929 (34579, Thermo Fisher Scientific) using the ChemiDoc XRS+ system (Bio-Rad). ImageLab
930 software was used to quantify the bands. Antibodies used in Western blot analysis are provided
931 in Supplementary Table 1.

932 ***Proliferation assay (MTT)***

933 5,000 cells/well were seeded in a 96-well plate to assess the proliferation of cells after METTL3
934 inhibitor STM2457 (10 µM) at indicated time points. CellTiter 96 Non-Radioactive Cell
935 Proliferation Assay kit (G4000, Promega) was used to determine cell growth and the
936 manufacturer's instructions were followed. Absorbance was measured using a microplate
937 reader Infinite 50 (Tecan, Austria).

938 **Drug treatments:**

939 U-2 OS cells were treated with Bleomycin 10 µg/ml containing media for 4 h. U-2 OS cells
940 were treated with Actinomycin D (10 µg/ml) for the indicated time points and RNA was
941 isolated from the treated cells to perform TERRA slot blot assay. METTL3 inhibitor STM2457

942 (10 μM, HY-134836), UZH1A (50 μM, HY-134673A), and UZH1B (50 μM, HY-134673B)
943 were treated for 6 h to perform TERRA RNA-FISH and 48 h for telomere DNA damage IF.
944 ***Colony formation assay***
945 10,000 cells/well were seeded in a 6-well plate and allowed to attach overnight. Doxycycline
946 (200 ng/ml) was added to the media for induction of METTL3-KD and cells were left to grow
947 sparsely for 14 days with induction media which was replaced after every 3-4 days. Cells were
948 then washed 1x with PBS, fixed with 4% formaldehyde for 10 min at RT, washed 1x with PBS,
949 and then stained using 1% crystal violet solution at RT for 2 h. The plate was carefully washed
950 and allowed to dry. The image was taken using the ChemiDoc XRS+ system (Bio-Rad).
951 ***In-vitro METTL3/METTL14 methyltransferase assay***
952 Methyl-transferase assay with RNA oligos (1 μm DRACH motif containing and TERRA repeat
953 containing oligo, Supplementary Table 1) was performed with recombinant
954 METTL3/METTL14 enzyme complex (31570, Active motif) according to manufacturer's
955 instructions, with 10 nM S-Adenosyl methionine (SAM) as methyl group donor. Oligos
956 without enzyme complex were used as a negative control. To detect if the RNA oligos
957 underwent m^6A modification LC-MS/MS-based quantification of m^6A was done, as previously
958 described (Liu et al. 2020). In brief oligos, post methyltransferase assay were digested by
959 Nuclease P1 (N8630, Sigma-Aldrich) followed by treatment with phosphatase (M0289S,
960 NEB). The sample was then filtered (0.22 μm pore size) and directly injected into the LC-MS.
961 We made triplicate injections of the RNA oligos (both experimental and negative controls) and
962 estimated the ratio of A/m^6A. LC-MS/MS profiles were monitored using the parallel reaction-
963 monitoring (PRM) mode for: m/z 268.0–136.0, m/z 282.0–150.1 which corresponds to A and
964 m^6A respectively as described before (Sun et al. 2021). DRACH oligos served as a positive
965 control.
966 **Purification of TERRA RNA and RNA-MS**
967 ***TERRA RNA pulldown***: Capturing a specific RNA from total RNA was performed as
968 described previously (55). In brief, ~300 μg of DNase I treated RNA isolated from U2O-S cells
969 was mixed with 400 pmoles of biotinylated DNA probe (Supplementary Table S1) against
970 TERRA or Luciferase probe (negative control) in 5x SSC buffer and denatured at 90°C for 3
971 min. This mixture was immediately cooled down on the ice and again heated at 65°C for 10
972 min after which the samples were left to cool down at RT to allow hybridization of the
973 probe. To pulldown the RNA hybridized with biotinylated DNA probes, MyOne Streptavidin
974 C1 magnetic Dynabeads (Thermo Fisher Scientific) were added and incubated for 30 min at
975 room temperature. The magnetic beads were washed once with 1x SSC buffer and thrice with

976 0.1x SSC buffer. To elute the captured RNA, the magnetic beads were resuspended in nuclease-
977 free water, and heated at 75°C for 3 min. The eluted RNA was treated with RNase-free DNase
978 I for 30 min at 37°C. Finally, the RNA was precipitated with 3 volumes of 100% ethanol, 0.5
979 M ammonium acetate, and GlycoBlue (Thermo Fisher Scientific) at -80°C for 2 h. The
980 precipitated RNA was washed with 80% ethanol and resuspended in nuclease-free water.
981 The RNA captured using TERRA or Luciferase probe (Luciferase) was first checked for
982 specificity by a slot blot assay using TERRA probe (see slot blot assay).
983 Further, the captured TERRA RNA along with synthetic RNA oligo (Supplementary Table S1)
984 were digested with RNase T1 and analyzed on a mass spectrometer (MS).
985 ***RNA-MS analysis**:* RNA-MS was performed using an Easy-nLC 1200 LC system (Thermo
986 Fisher Scientific) coupled to Orbitrap Fusion™ Eclipse™ Tribrid™ mass spectrometer. The
987 analytes were trapped on a 2 cm x 100 µm Acclaim PepMap C18 precolumn (particle size
988 5 µm; Thermo Fisher Scientific) and separated on a 30 cm x 75 µm analytical column packed
989 in-house with 3 µm Reprosil-Pur C18 material (Dr. Maisch, Germany) at 300 nL/min flow
990 using a stepwise elution profile during 45 min. Solvent A was 5 mM di-n-butylamine and 8 mM
991 acetic acid in H_2O, and solvent B was 70% methanol, 5 mM di-n-butylamine, and 8 mM acetic
992 acid. The column oven temperature was 50°C. Nano-Flex ion source (Thermo Fisher
993 Scientific) was operated in negative ionization mode at 1.8 kV with the ion transfer capillary
994 temperature 275°C. The MS instrument was run in a targeted MS/MS setting with switching
995 quadrupole isolation between the two tetramers of interest. Each precursor was isolated with a
996 1.1 Da window and followed by HCD 30% recorded at 15,000 resolution in the Orbitrap with
997 the first m/z 130. The monoisotopic mass of UUAGp is 1304.1 Da equivalent to doubly charged
998 m/z 651.07 and UUm^{6}AGp has a monoisotopic mass of UUAGp is 1318.2 Da equivalent to
999 doubly charged m/z 658.08. The ratio of UUm^{6}AGp over UUAGp was calculated from the
1000 average intensities of the respective fragment ions. The MS2 spectra over the targeted
1001 precursors for 30 seconds were averaged and the total fragment intensities were calculated and
1002 compared. The intensities for UUm^{6}AGp fragment ions were divided by the total sum of
1003 UUAGp and UUm^{6}AGp fragment ions intensities.
1004 ***METTL3 Chromatin Immunoprecipitation (ChIP)***
1005 ChIP with METTL3 antibody was performed as described before (70). U-2 OS cells were fixed
1006 with formaldehyde (1% final concentration) for 15 min at RT. Fixed cells were washed with
1007 cold PBS, lysed and the chromatin was sheared using a Bioruptor (Diagenode) until an average
1008 fragment size range of 200-500 bp was achieved. Immunoprecipitation of solubilized
1009 chromatin was carried out with 3 µg of METTL3/IgG antibody overnight at 4°C. The

1010 immunoprecipitated complex was captured using a mix of Protein A and G Dynabeads
1011 (Invitrogen), washed and RNase A treated before eluting the DNA. The ChIP DNA was
1012 denatured at 95°C for 5 min before assaying on slot blot using TERRA probe.

1013 ***Re-RIP (hnRNPA2B1-m^{6}A)***

1014 Control-sh and METTL3-KD U-2 OS cells were harvested and fixed for 10 min with
1015 formaldehyde (1% final concentration) and quenched with Glycine (0.125 M, final
1016 concentration). Fixed cells were lysed in RIPA buffer (50 mM Tris pH7.4, 150 mM NaCl, 0.5%
1017 Sodium Deoxycholate, 0.2% SDS, 1% IGEPAL-CA630, Protease inhibitor, and RNase
1018 inhibitor) and sonicated for 10 cycles (30 secs on 30 secs off) on Bioruptor (Diagenode) and
1019 cleared lysate was used for RIP with 3 µg of hnRNPA2B1 (A73256, Gentek,) and IgG (sc-
1020 2027, Santa Cruz) antibodies. The RNA-protein-antibody complex was captured using protein
1021 A/G magnetic beads (Thermo Fisher Scientific). Magnetic beads were washed with low salt
1022 buffer (1x PBS, 0.1% SDS, and 0.5% IGEPAL-CA630) and high salt buffer (5x PBS, 0.1%
1023 SDS, and 0.5% IGEPAL-CA630) before eluting in elution buffer (10 mM Tris pH 7.4, 100
1024 mM NaCl, 1 mM EDTA, 0.5% SDS) with Proteinase K followed by RNA extraction using
1025 TRIzol reagent. The RNA isolated after hnRNPA2B1/IgG RIP was subsequently used as input
1026 for Re-RIP with m^{6}A antibody. m^{6}A RIP was performed as described in the above section.
1027 The final Re-RIP RNA was directly assayed on slot blot.

1028 **Purification of hnRNPA2B1 protein and *in vitro* binding assay**

1029 His-tagged hnRNPA2_WT (98662, Addgene) was transformed in Rossetta DE3 bacterial
1030 strain. Cells were grown overnight and further diluted to 0.1 OD 600 nm and grown to about
1031 0.6 OD 600 nm at 37°C and then cells were induced with 0.3 mM IPTG at 18°C for 14-16 h.
1032 Cells were pelleted and dissolved in 25 mM HEPES pH 7.5, 150 mM NaCl, 20 mM KCl, and
1033 20 mM $MgCl_2$ along with 1x Protease inhibitor cocktail. Cells were lysed at 4°C in presence
1034 of lysozyme followed by brief sonication. Cells debris were removed by spinning cells lysate
1035 at 13000 rpm for 30 min at 4C and cleared lysate were loaded onto Co+ NTA resin for binding
1036 of His-tagged hnRNPA2B1 protein and resin were washed with 20 mM imidazole containing
1037 lysis buffer without 1x Protease inhibitor cocktail to remove non-specific proteins and His-
1038 tagged protein were eluted in 300 mM imidazole containing lysis buffer and eluted protein
1039 were further dialyzed in lysis buffer and proteins were stored in -80°C for further use.

1040 The hnRNPA2B1 binding with RNA was performed following the protocol as described before
1041 (71) with few modifications. Total RNA from Control-sh or METTL3-KD U-2 OS cells were
1042 used instead of *in vitro* synthesized RNA. The RNA bound protein complex was captured by

1043 HisPur Cobalt Resin (89965, Thermo Fisher Scientific) and TERRA enrichment was checked
1044 by slot blot assay as described above.

1045 ***Analysis associated with detection of Chromosomal aberration and ATRX status in NB***
1046 ***Swedish cohort***

1047 Tumor samples were analyzed with Applied biosystems CytoScan HD array (Thermo Fisher
1048 Scientific, Waltham) according to the experimental procedure previously described (72,73).
1049 The arrays detect both copy number alterations and allele-specific information at high
1050 resolution. For primary data analysis, GDAS software (Thermo Fisher Scientific) was used.
1051 Chromosome Analysis Suite (ChAS v.3.3; Thermo Fisher Scientific) was used for the
1052 generation of genomic profiles and determination of chromosomal aberration, MYCN
1053 amplification, and ATRX status. For Whole Genome Sequencing (WGS) DNA from tumor
1054 material and matched constitutional DNA were subjected to sequencing and bioinformatical
1055 handling as described previously (73).

1056 ***C-circle assay***

1057 50 ng of genomic DNA was digested with 4 U/µg HinfI and RsaI restriction enzymes and 25
1058 ng/µg RNase for 1 h at 37°C (prepare every sample twice to include no polymerase as negative
1059 control). Digested DNA was incubated with 100ug/ml Albumin, 1 mM each dATP, dGTP, and
1060 dTTP, 0.1% Tween, 1x Φ29 Buffer, and 7.5 U Φ29 DNA polymerase (NEB) at 30°C for 8 h
1061 then 65°C for 20 min. The reaction products were slot blotted onto a 6x SSC soaked Biodyne
1062 B nylon membrane (GE Healthcare) for quantification and UV-crosslinking the DNA onto the
1063 membrane at 0.120 Joules. Prehybridization was done using DIG Easy Hyb (11603558001,
1064 Roche) for 30 min at 37°C, and after adding 25 ng/ml DIG-labeled TERRA probe: 5´-
1065 $(TAACCC)_5$-DIG (Sigma-Aldrich) at 37°C overnight with rotation. For hybridization, the DIG
1066 Wash and Block Buffer set (11585762001, Roche) was used according to the manufacturer's
1067 instructions. The membrane was incubated with an anti-DIG antibody conjugated with alkaline
1068 phosphatase (1:20,000, 11093274910, Roche) for 1 h and CDP-Star Chemoluminescent
1069 substrate (C0712, Sigma-Aldrich) to detect the C-circles. Images were taken using High-
1070 resolution Chemiluminescence (ChemiDoc, Bio-Rad)

1071 ***Telomere DNA FISH and Immunostaining***

1072 The cells were fixed with 4% formaldehyde for 10 min, followed two washes with PBS. Then,
1073 cells were permeabilized using 0.25% Triton X-100 in PBS for 10 min, followed by two washes
1074 with 0.1% PBS-Tween (PBS-T). Blocking step and RNase A treatment were performed by
1075 adding RNase A (100 µg/ml, Sigma-Aldrich) in 3% bovine serum albumin (BSA) for 1h at RT,

1076 followed by 2 washes with PBS-T. The cells were incubated overnight with primary antibody
1077 γ-H2AX (1:500, Thermo Fisher Scientific) at 4°C, washed three times 5 min in PBS-T, and
1078 subsequently incubated with secondary antibody conjugated with Alexa Fluor 555 (1:800,
1079 A32727, Thermo Fisher Scientific) for a 1 h in the dark at room temperature. After incubation
1080 with the antibody, cells were washed three times for 5 min in PBS-T. Following
1081 immunofluorescence staining, the cells were refixed using 4% formaldehyde for 10 min. After
1082 washing twice with PBS, the slides were dehydrated with 50, 70, and 100% ethanol for 3 min
1083 and air dried for 5 min at RT. For hybridization, denature slide with probe (1:200, $(TAACCC)_7$-
1084 Atto488) in hybridization buffer (20 mM Na_2HPO_4, pH 7.4, 20 mM Tris, pH 7.4, 60%
1085 formamide, 2x SSC and 0.1 µg/ml salmon sperm DNA) for 10 min at 85°C, and incubated with
1086 the probe in a humidified chamber for 2 h at RT. Following hybridization, wash twice in
1087 washing solution (2x SCC/0.1% Tween) for 15 min each and MQ water twice for 2 min.
1088 Prolong Gold with DAPI (Thermo Fisher Scientific) was added to each coverslip and air-dried
1089 in the dark before imaging using 60X objectives in EVOS M7000 microscope.

1090 ***Mouse xenograft experiments***

1091 TetO Control and METTL3-KD SK-N-F1 and CHLA-90 cells were subcutaneously injected
1092 into the right dorsal flank (2 x 10^6 and 5 × 10^6 cells, respectively) of 5-week-old female nude
1093 mice (Charles River) in 100 µL and 200 µL mixture of (1:3) Matrigel/PBS, (n=4 and 3 per
1094 group, respectively). METTL3 knockdown was induced by adding 2 mg/mL Dox and 2%
1095 sucrose to drinking water, after 4-5 days of cell injection. Mice weight was monitored weekly
1096 and tumor volume was measured every 2–3 days using a digital calliper and calculated
1097 according to the formula Volume (mm3) = (w2 x l x π)/6 (where w is width, shortest diameter,
1098 and l is length, longest diameter). Mice were euthanized when tumors reached 1000 mm3 or
1099 had weight loss ≥ 10% of initial weight. At the end of the experiment, tumors were collected,
1100 weighed, and processed for further analysis. All experiments were carried out per the standards
1101 approved by the Institutional Ethical Committee of Animal Experimentation, Gothenburg,
1102 Sweden (ethical permit no 3722/21). METTL3-KD was verified before and after cell injection
1103 by Western blot.

1104 ***DNA-RNA immunoprecipitation (DRIP) and DRIP followed by m^6A RIP (DRImR)***

1105 DRIP was performed as described previously with few alterations. In brief, cells were lysed in
1106 lysis buffer (1xTE supplemented with 0.5% SDS) for 15 min at RT. Brief RNase A treatment
1107 at 37°C for 15 min was done to remove free RNA from the subsequent Proteinase K treatment
1108 and genomic DNA isolation by Phenol chloroform isolation. The genomic DNA before S9.6

1109 IP were digested with a cocktail of restriction enzymes (*Bsr*GI, *Eco*RI, *Hind*III, *Ssp*I, and *Xba*I)
1110 and RNase III which is shown to remove non-specific enrichment of double-stranded RNA to
1111 identify genuine R-loop enriched RNAs. IP reaction was carried out with fragmented genomic
1112 DNA that was either pre-treated/non-pre-treated with RNase H to cross-check the specificity
1113 of S9.6 IP. Following 9.6 IP we performed extensive DNase I treatment to obtain R-loop
1114 associated RNA. For DRImR, DRIP enriched RNA was used as input for m^6A RIP as described
1115 above with above without fragmentation.

1116 ***Analysis of neuroblastoma next-generation sequencing data from a German cohort***

1117

1118 Copy number gains were estimated from a combination of published neuroblastoma paired-
1119 end WGS (25) paired-end WES (26), and aCGH (74) datasets. ALT and MYCN status of the
1120 patients were taken from sample overlaps with Roderweiser et al. (46), sequence alignment to
1121 reference GRCh37/hg19 was done using BWA mem (v.0.7.13-r1126;
1122 https://github.com/lh3/bwa) and copy number analysis was performed with Sclust(75).
1123 Gene expression analysis was performed with the RNA-Seq dataset published by Zhang et al
1124 (76). Expression values had been computed using the Magic-AceView pipeline and were given
1125 as normalized log(sFPKM) values [see (46) for details]. Survival information, ALT, and
1126 MYCN annotation were again taken from Roderweiser et al. (46). Survival analysis was done
1127 with groups with high and low expression of selected genes in survival analysis were generated
1128 by maximally selected rank statistics using the R package maxstat (version 0.7-25).

1129

1130 ***Image quantification and statistical analysis:***

1131 Western and slot blots were quantified using ImageLab software (Bio-Rad). Images were
1132 quantified using ImageJ software (77). DAPI was used to mark the nuclear border and TERRA
1133 foci, PLA foci, or colocalization signals within the nucleus were counted using particle
1134 analysis. More than 100 nuclei were counted for U-2 OS cells and at least 50 nuclei in the case
1135 of NB cells for each experiment. Graphs were prepared, and statistical analysis was performed
1136 using GraphPad Prism (version 9.4.1 for Windows, GraphPad Software, San Diego, California,
1137 USA, www.graphpad.com). The data are displayed as Mean ± Standard Deviation (SD) of a
1138 minimum of three independent experiments. Each box-and-whisker plot presents the median
1139 value as a line, a box around the lower and higher quartiles, and whiskers extending to the
1140 maximum and lowest values. Statistical significance between 2 groups was analyzed by
1141 Student's 2-tailed unpaired t-test. Wilcoxon paired signed-rank test, Dunnett's test, Turkey's

test, and Sidak's test were used to perform multiple comparisons, and *p*-values were reported in the Figures and the Figure legends.

Data availability

The data underlying this article are available in NCBI Gene Expression Omnibus (GEO) at https://www.ncbi.nlm.nih.gov/geo/ and can be accessed with the GSE219146 and GSE219212 accession numbers.

Acknowledgements

We would like to thank the core facility at Novum, BEA, Bioinformatics and Expression Analysis, which is supported by the board of research at the Karolinska Institute and the research committee at the Karolinska hospital for help with sequencing. Proteomics core facility at GU for their support with LC-MS/MS. The computations and data handling were enabled by resources in project SNIC-2022-22-85 provided by the Swedish National Infrastructure for Computing (SNIC) at UPPMAX, partially funded by the Swedish Council through grant agreement no. 2018-05973. We acknowledge Anders Sjölander for assistance concerning technical and implementational aspects of the UPPMAX resources.

Funding:

This work was funded by grants from the Swedish Research Council (Vetenskapsrådet, 2018-02224) and project grants from Svenska Läkaresällskapet, Barncancerfonden, Cancerfonden, Åke Wibergs Stiftelse, and Kungl Vetenskaps- och Vitterhets-Samhället (KVVS) grant to TM, 4 years research position grant from Barncancerfonden to TM, Tore Nilsons Stiftelse and Bollan scholarship to RV, Assar Gabrielsson Fond to RV and KT.

References:

1. Barbieri, I. and Kouzarides, T. (2020) Role of RNA modifications in cancer. *Nat Rev Cancer*, **20**, 303-322.
2. Huang, H., Weng, H., Zhou, K., Wu, T., Zhao, B.S., Sun, M., Chen, Z., Deng, X., Xiao, G., Auer, F. *et al.* (2019) Histone H3 trimethylation at lysine 36 guides m(6)A RNA modification co-transcriptionally. *Nature*, **567**, 414-419.
3. Patil, D.P., Chen, C.K., Pickering, B.F., Chow, A., Jackson, C., Guttman, M. and Jaffrey, S.R. (2016) m(6)A RNA methylation promotes XIST-mediated transcriptional repression. *Nature*, **537**, 369-373.
4. Yue, Y., Liu, J., Cui, X., Cao, J., Luo, G., Zhang, Z., Cheng, T., Gao, M., Shu, X., Ma, H. *et al.* (2018) VIRMA mediates preferential m(6)A mRNA methylation in 3'UTR and near stop codon and associates with alternative polyadenylation. *Cell Discov*, **4**, 10.
5. Xu, W., Li, J., He, C., Wen, J., Ma, H., Rong, B., Diao, J., Wang, L., Wang, J., Wu, F. *et al.* (2021) METTL3 regulates heterochromatin in mouse embryonic stem cells. *Nature*, **591**, 317-321.

1179 6. Zheng, G., Dahl, J.A., Niu, Y., Fedorcsak, P., Huang, C.M., Li, C.J., Vagbo, C.B., Shi, Y.,
1180 Wang, W.L., Song, S.H. *et al.* (2013) ALKBH5 is a mammalian RNA demethylase that
1181 impacts RNA metabolism and mouse fertility. *Mol Cell*, **49**, 18-29.
1182 7. Alarcon, C.R., Goodarzi, H., Lee, H., Liu, X., Tavazoie, S. and Tavazoie, S.F. (2015)
1183 HNRNPA2B1 Is a Mediator of m(6)A-Dependent Nuclear RNA Processing Events. *Cell*,
1184 **162**, 1299-1308.
1185 8. Zhou, K.I., Shi, H., Lyu, R., Wylder, A.C., Matuszek, Z., Pan, J.N., He, C., Parisien, M. and
1186 Pan, T. (2019) Regulation of Co-transcriptional Pre-mRNA Splicing by m(6)A through
1187 the Low-Complexity Protein hnRNPG. *Mol Cell*, **76**, 70-81 e79.
1188 9. Xu, W., He, C., Kaye, E.G., Li, J., Mu, M., Nelson, G.M., Dong, L., Wang, J., Wu, F., Shi,
1189 Y.G. *et al.* (2022) Dynamic control of chromatin-associated m(6)A methylation
1190 regulates nascent RNA synthesis. *Mol Cell*, **82**, 1156-1168 e1157.
1191 10. Liu, J., Gao, M., He, J., Wu, K., Lin, S., Jin, L., Chen, Y., Liu, H., Shi, J., Wang, X. *et al.*
1192 (2021) The RNA m(6)A reader YTHDC1 silences retrotransposons and guards ES cell
1193 identity. *Nature*, **591**, 322-326.
1194 11. Abakir, A., Giles, T.C., Cristini, A., Foster, J.M., Dai, N., Starczak, M., Rubio-Roldan, A.,
1195 Li, M., Eleftheriou, M., Crutchley, J. *et al.* (2020) N(6)-methyladenosine regulates the
1196 stability of RNA:DNA hybrids in human cells. *Nat Genet*, **52**, 48-55.
1197 12. Yang, X., Liu, Q.L., Xu, W., Zhang, Y.C., Yang, Y., Ju, L.F., Chen, J., Chen, Y.S., Li, K., Ren,
1198 J. *et al.* (2019) m(6)A promotes R-loop formation to facilitate transcription
1199 termination. *Cell Res*, **29**, 1035-1038.
1200 13. Porman, A.M., Roberts, J.T., Duncan, E.D., Chrupcala, M.L., Levine, A.A., Kennedy,
1201 M.A., Williams, M.M., Richer, J.K. and Johnson, A.M. (2022) A single N6-
1202 methyladenosine site regulates lncRNA HOTAIR function in breast cancer cells. *PLoS*
1203 *Biol*, **20**, e3001885.
1204 14. Wang, X., Liu, C., Zhang, S., Yan, H., Zhang, L., Jiang, A., Liu, Y., Feng, Y., Li, D., Guo, Y.
1205 *et al.* (2021) N(6)-methyladenosine modification of MALAT1 promotes metastasis via
1206 reshaping nuclear speckles. *Dev Cell*, **56**, 702-715 e708.
1207 15. Jones, A.N., Tikhaia, E., Mourao, A. and Sattler, M. (2022) Structural effects of m6A
1208 modification of the Xist A-repeat AUCG tetraloop and its recognition by YTHDC1.
1209 *Nucleic Acids Res*, **50**, 2350-2362.
1210 16. Ninomiya, K., Iwakiri, J., Aly, M.K., Sakaguchi, Y., Adachi, S., Natsume, T., Terai, G., Asai,
1211 K., Suzuki, T. and Hirose, T. (2021) m(6) A modification of HSATIII lncRNAs regulates
1212 temperature-dependent splicing. *EMBO J*, **40**, e107976.
1213 17. Liu, J., Dou, X., Chen, C., Chen, C., Liu, C., Xu, M.M., Zhao, S., Shen, B., Gao, Y., Han, D.
1214 *et al.* (2020) N (6)-methyladenosine of chromosome-associated regulatory RNA
1215 regulates chromatin state and transcription. *Science*, **367**, 580-586.
1216 18. Lee, J.H., Wang, R., Xiong, F., Krakowiak, J., Liao, Z., Nguyen, P.T., Moroz-Omori, E.V.,
1217 Shao, J., Zhu, X., Bolt, M.J. *et al.* (2021) Enhancer RNA m6A methylation facilitates
1218 transcriptional condensate formation and gene activation. *Mol Cell*, **81**, 3368-3385
1219 e3369.
1220 19. Azzalin, C.M., Reichenbach, P., Khoriauli, L., Giulotto, E. and Lingner, J. (2007)
1221 Telomeric repeat containing RNA and RNA surveillance factors at mammalian
1222 chromosome ends. *Science*, **318**, 798-801.
1223 20. Schoeftner, S. and Blasco, M.A. (2008) Developmentally regulated transcription of
1224 mammalian telomeres by DNA-dependent RNA polymerase II. *Nat Cell Biol*, **10**, 228-
1225 236.

1226 21. Feretzaki, M., Pospisilova, M., Valador Fernandes, R., Lunardi, T., Krejci, L. and Lingner,
1227 J. (2020) RAD51-dependent recruitment of TERRA lncRNA to telomeres through R-
1228 loops. *Nature*, **587**, 303-308.
1229 22. Vohhodina, J., Goehring, L.J., Liu, B., Kong, Q., Botchkarev, V.V., Jr., Huynh, M., Liu, Z.,
1230 Abderazzaq, F.O., Clark, A.P., Ficarro, S.B. *et al.* (2021) BRCA1 binds TERRA RNA and
1231 suppresses R-Loop-based telomeric DNA damage. *Nat Commun*, **12**, 3542.
1232 23. Giannone, R.J., McDonald, H.W., Hurst, G.B., Shen, R.F., Wang, Y. and Liu, Y. (2010)
1233 The protein network surrounding the human telomere repeat binding factors TRF1,
1234 TRF2, and POT1. *PLoS One*, **5**, e12407.
1235 24. Yoshida, A., Oyoshi, T., Suda, A., Futaki, S. and Imanishi, M. (2022) Recognition of G-
1236 quadruplex RNA by a crucial RNA methyltransferase component, METTL14. *Nucleic*
1237 *Acids Res*, **50**, 449-457.
1238 25. Peifer, M., Hertwig, F., Roels, F., Dreidax, D., Gartlgruber, M., Menon, R., Kramer, A.,
1239 Roncaioli, J.L., Sand, F., Heuckmann, J.M. *et al.* (2015) Telomerase activation by
1240 genomic rearrangements in high-risk neuroblastoma. *Nature*, **526**, 700-704.
1241 26. Ackermann, S., Cartolano, M., Hero, B., Welte, A., Kahlert, Y., Roderwieser, A.,
1242 Bartenhagen, C., Walter, E., Gecht, J., Kerschke, L. *et al.* (2018) A mechanistic
1243 classification of clinical phenotypes in neuroblastoma. *Science*, **362**, 1165-1170.
1244 27. Koneru, B., Lopez, G., Farooqi, A., Conkrite, K.L., Nguyen, T.H., Macha, S.J., Modi, A.,
1245 Rokita, J.L., Urias, E., Hindle, A. *et al.* (2020) Telomere Maintenance Mechanisms
1246 Define Clinical Outcome in High-Risk Neuroblastoma. *Cancer Res*, **80**, 2663-2675.
1247 28. Macha, S.J., Koneru, B., Burrow, T.A., Zhu, C., Savitski, D., Rahman, R.L., Ronaghan,
1248 C.A., Nance, J., McCoy, K., Eslinger, C. *et al.* (2022) Alternative Lengthening of
1249 Telomeres in Cancer Confers a Vulnerability to Reactivation of p53 Function. *Cancer*
1250 *Res*, **82**, 3345-3358.
1251 29. Sun, H., Li, K., Zhang, X., Liu, J., Zhang, M., Meng, H. and Yi, C. (2021) m(6)Am-seq
1252 reveals the dynamic m(6)Am methylation in the human transcriptome. *Nat Commun*,
1253 **12**, 4778.
1254 30. Fu, Y. and Zhuang, X. (2020) m(6)A-binding YTHDF proteins promote stress granule
1255 formation. *Nat Chem Biol*, **16**, 955-963.
1256 31. Nurk, S., Koren, S., Rhie, A., Rautiainen, M., Bzikadze, A.V., Mikheenko, A., Vollger,
1257 M.R., Altemose, N., Uralsky, L., Gershman, A. *et al.* (2022) The complete sequence of
1258 a human genome. *Science*, **376**, 44-53.
1259 32. Deng, Z., Wang, Z., Stong, N., Plasschaert, R., Moczan, A., Chen, H.S., Hu, S.,
1260 Wikramasinghe, P., Davuluri, R.V., Bartolomei, M.S. *et al.* (2012) A role for CTCF and
1261 cohesin in subtelomere chromatin organization, TERRA transcription, and telomere
1262 end protection. *EMBO J*, **31**, 4165-4178.
1263 33. Zeng, Y., Wang, S., Gao, S., Soares, F., Ahmed, M., Guo, H., Wang, M., Hua, J.T., Guan,
1264 J., Moran, M.F. *et al.* (2018) Refined RIP-seq protocol for epitranscriptome analysis
1265 with low input materials. *PLoS Biol*, **16**, e2006092.
1266 34. Chen, L., Zhang, C., Ma, W., Huang, J., Zhao, Y. and Liu, H. (2022) METTL3-mediated
1267 m6A modification stabilizes TERRA and maintains telomere stability. *Nucleic Acids Res*.
1268 35. Pratanwanich, P.N., Yao, F., Chen, Y., Koh, C.W.Q., Wan, Y.K., Hendra, C., Poon, P., Goh,
1269 Y.T., Yap, P.M.L., Chooi, J.Y. *et al.* (2021) Identification of differential RNA
1270 modifications from nanopore direct RNA sequencing with xPore. *Nat Biotechnol*, **39**,
1271 1394-1402.

1272 36. Tan, K.T., Slevin, M.K., Meyerson, M. and Li, H. (2022) Identifying and correcting
1273 repeat-calling errors in nanopore sequencing of telomeres. *Genome Biol*, **23**, 180.
1274 37. Zhang, C., Chen, L., Peng, D., Jiang, A., He, Y., Zeng, Y., Xie, C., Zhou, H., Luo, X., Liu, H.
1275 *et al.* (2020) METTL3 and N6-Methyladenosine Promote Homologous Recombination-
1276 Mediated Repair of DSBs by Modulating DNA-RNA Hybrid Accumulation. *Mol Cell*, **79**,
1277 425-442 e427.
1278 38. Xiang, Y., Laurent, B., Hsu, C.H., Nachtergaele, S., Lu, Z., Sheng, W., Xu, C., Chen, H.,
1279 Ouyang, J., Wang, S. *et al.* (2017) RNA m(6)A methylation regulates the ultraviolet-
1280 induced DNA damage response. *Nature*, **543**, 573-576.
1281 39. Liu, M., Hales, B.F. and Robaire, B. (2014) Effects of four chemotherapeutic agents,
1282 bleomycin, etoposide, cisplatin, and cyclophosphamide, on DNA damage and
1283 telomeres in a mouse spermatogonial cell line. *Biol Reprod*, **90**, 72.
1284 40. Xiong, F., Wang, R., Lee, J.H., Li, S., Chen, S.F., Liao, Z., Hasani, L.A., Nguyen, P.T., Zhu,
1285 X., Krakowiak, J. *et al.* (2021) RNA m(6)A modification orchestrates a LINE-1-host
1286 interaction that facilitates retrotransposition and contributes to long gene
1287 vulnerability. *Cell Res*, **31**, 861-885.
1288 41. Xu, M., Chigumira, T., Chen, Z., Tones, J., Zhao, R., Dahl, K.N., Chenoweth, D.M. and
1289 Zhang, H. (2021) CRISPR Cas13-Based Tools to Track and Manipulate Endogenous
1290 Telomeric Repeat-Containing RNAs in Live Cells. *Front Mol Biosci*, **8**, 785160.
1291 42. Yankova, E., Blackaby, W., Albertella, M., Rak, J., De Braekeleer, E., Tsagkogeorga, G.,
1292 Pilka, E.S., Aspris, D., Leggate, D., Hendrick, A.G. *et al.* (2021) Small-molecule inhibition
1293 of METTL3 as a strategy against myeloid leukaemia. *Nature*, **593**, 597-601.
1294 43. Moroz-Omori, E.V., Huang, D., Kumar Bedi, R., Cheriyamkunnel, S.J., Bochenkova, E.,
1295 Dolbois, A., Rzeczkowski, M.D., Li, Y., Wiedmer, L. and Caflisch, A. (2021) METTL3
1296 Inhibitors for Epitranscriptomic Modulation of Cellular Processes. *ChemMedChem*, **16**,
1297 3035-3043.
1298 44. Chu, H.P., Cifuentes-Rojas, C., Kesner, B., Aeby, E., Lee, H.G., Wei, C., Oh, H.J., Boukhali,
1299 M., Haas, W. and Lee, J.T. (2017) TERRA RNA Antagonizes ATRX and Protects
1300 Telomeres. *Cell*, **170**, 86-101 e116.
1301 45. Hartono, S.R., Malapert, A., Legros, P., Bernard, P., Chedin, F. and Vanoosthuyse, V.
1302 (2018) The Affinity of the S9.6 Antibody for Double-Stranded RNAs Impacts the
1303 Accurate Mapping of R-Loops in Fission Yeast. *J Mol Biol*, **430**, 272-284.
1304 46. Roderwieser, A., Sand, F., Walter, E., Fischer, J., Gecht, J., Bartenhagen, C., Ackermann,
1305 S., Otte, F., Welte, A., Kahlert, Y. *et al.* (2019) Telomerase Is a Prognostic Marker of
1306 Poor Outcome and a Therapeutic Target in Neuroblastoma. *JCO Precis Oncol*, **3**, 1-20.
1307 47. Hartlieb, S.A., Sieverling, L., Nadler-Holly, M., Ziehm, M., Toprak, U.H., Herrmann, C.,
1308 Ishaque, N., Okonechnikov, K., Gartlgruber, M., Park, Y.G. *et al.* (2021) Alternative
1309 lengthening of telomeres in childhood neuroblastoma from genome to proteome. *Nat*
1310 *Commun*, **12**, 1269.
1311 48. Porro, A., Feuerhahn, S., Reichenbach, P. and Lingner, J. (2010) Molecular dissection
1312 of telomeric repeat-containing RNA biogenesis unveils the presence of distinct and
1313 multiple regulatory pathways. *Mol Cell Biol*, **30**, 4808-4817.
1314 49. Wu, B., Su, S., Patil, D.P., Liu, H., Gan, J., Jaffrey, S.R. and Ma, J. (2018) Molecular basis
1315 for the specific and multivariant recognitions of RNA substrates by human hnRNP
1316 A2/B1. *Nat Commun*, **9**, 420.
1317 50. Martinez, F.J., Pratt, G.A., Van Nostrand, E.L., Batra, R., Huelga, S.C., Kapeli, K., Freese,
1318 P., Chun, S.J., Ling, K., Gelboin-Burkhart, C. *et al.* (2016) Protein-RNA Networks

1319 Regulated by Normal and ALS-Associated Mutant HNRNPA2B1 in the Nervous System.
1320 *Neuron*, **92**, 780-795.
1321 51. Linder, B., Grozhik, A.V., Olarerin-George, A.O., Meydan, C., Mason, C.E. and Jaffrey,
1322 S.R. (2015) Single-nucleotide-resolution mapping of m6A and m6Am throughout the
1323 transcriptome. *Nat Methods*, **12**, 767-772.
1324 52. Petti, E., Buemi, V., Zappone, A., Schillaci, O., Broccia, P.V., Dinami, R., Matteoni, S.,
1325 Benetti, R. and Schoeftner, S. (2019) SFPQ and NONO suppress RNA:DNA-hybrid-
1326 related telomere instability. *Nat Commun*, **10**, 1001.
1327 53. Nguyen, E.D., Balas, M.M., Griffin, A.M., Roberts, J.T. and Johnson, A.M. (2018) Global
1328 profiling of hnRNP A2/B1-RNA binding on chromatin highlights LncRNA interactions.
1329 *RNA Biol*, **15**, 901-913.
1330 54. Liu, N., Dai, Q., Zheng, G., He, C., Parisien, M. and Pan, T. (2015) N(6)-
1331 methyladenosine-dependent RNA structural switches regulate RNA-protein
1332 interactions. *Nature*, **518**, 560-564.
1333 55. Duda, K.J., Ching, R.W., Jerabek, L., Shukeir, N., Erikson, G., Engist, B., Onishi-
1334 Seebacher, M., Perrera, V., Richter, F., Mittler, G. *et al.* (2021) m6A RNA methylation
1335 of major satellite repeat transcripts facilitates chromatin association and RNA:DNA
1336 hybrid formation in mouse heterochromatin. *Nucleic Acids Res*, **49**, 5568-5587.
1337 56. Montero, J.J., Lopez-Silanes, I., Megias, D., M, F.F., Castells-Garcia, A. and Blasco, M.A.
1338 (2018) TERRA recruitment of polycomb to telomeres is essential for histone
1339 trymethylation marks at telomeric heterochromatin. *Nat Commun*, **9**, 1548.
1340 57. Kim, D., Paggi, J.M., Park, C., Bennett, C. and Salzberg, S.L. (2019) Graph-based genome
1341 alignment and genotyping with HISAT2 and HISAT-genotype. *Nat Biotechnol*, **37**, 907-
1342 915.
1343 58. Tarasov, A., Vilella, A.J., Cuppen, E., Nijman, I.J. and Prins, P. (2015) Sambamba: fast
1344 processing of NGS alignment formats. *Bioinformatics*, **31**, 2032-2034.
1345 59. Heinz, S., Benner, C., Spann, N., Bertolino, E., Lin, Y.C., Laslo, P., Cheng, J.X., Murre, C.,
1346 Singh, H. and Glass, C.K. (2010) Simple combinations of lineage-determining
1347 transcription factors prime cis-regulatory elements required for macrophage and B
1348 cell identities. *Mol Cell*, **38**, 576-589.
1349 60. Ramirez, F., Dundar, F., Diehl, S., Gruning, B.A. and Manke, T. (2014) deepTools: a
1350 flexible platform for exploring deep-sequencing data. *Nucleic Acids Res*, **42**, W187-
1351 191.
1352 61. Lawrence, M., Gentleman, R. and Carey, V. (2009) rtracklayer: an R package for
1353 interfacing with genome browsers. *Bioinformatics*, **25**, 1841-1842.
1354 62. Kent, W.J., Zweig, A.S., Barber, G., Hinrichs, A.S. and Karolchik, D. (2010) BigWig and
1355 BigBed: enabling browsing of large distributed datasets. *Bioinformatics*, **26**, 2204-
1356 2207.
1357 63. Li, H. (2018) Minimap2: pairwise alignment for nucleotide sequences. *Bioinformatics*,
1358 **34**, 3094-3100.
1359 64. Li, H. (2021) New strategies to improve minimap2 alignment accuracy. *Bioinformatics*,
1360 **37**, 4572-4574.
1361 65. Kovaka, S., Zimin, A.V., Pertea, G.M., Razaghi, R., Salzberg, S.L. and Pertea, M. (2019)
1362 Transcriptome assembly from long-read RNA-seq alignments with StringTie2. *Genome*
1363 *Biol*, **20**, 278.
1364 66. Lee, S., Cook, D. and Lawrence, M. (2019) plyranges: a grammar of genomic data
1365 transformation. *Genome Biol*, **20**, 4.

1366 67. Pockrandt, C., Alzamel, M., Iliopoulos, C.S. and Reinert, K. (2020) GenMap: ultra-fast
1367 computation of genome mappability. *Bioinformatics*, **36**, 3687-3692.
1368 68. Quinlan, A.R. and Hall, I.M. (2010) BEDTools: a flexible suite of utilities for comparing
1369 genomic features. *Bioinformatics*, **26**, 841-842.
1370 69. Feuerbach, L., Sieverling, L., Deeg, K.I., Ginsbach, P., Hutter, B., Buchhalter, I.,
1371 Northcott, P.A., Mughal, S.S., Chudasama, P., Glimm, H. *et al.* (2019) TelomereHunter
1372 - in silico estimation of telomere content and composition from cancer genomes. *BMC*
1373 *Bioinformatics*, **20**, 272.
1374 70. Vaid, R., Wen, J. and Mannervik, M. (2020) Release of promoter-proximal paused Pol
1375 II in response to histone deacetylase inhibition. *Nucleic Acids Res*, **48**, 4877-4890.
1376 71. Mondal, T., Subhash, S., Vaid, R., Enroth, S., Uday, S., Reinius, B., Mitra, S.,
1377 Mohammed, A., James, A.R., Hoberg, E. *et al.* (2015) MEG3 long noncoding RNA
1378 regulates the TGF-beta pathway genes through formation of RNA-DNA triplex
1379 structures. *Nat Commun*, **6**, 7743.
1380 72. Caren, H., Kryh, H., Nethander, M., Sjoberg, R.M., Trager, C., Nilsson, S., Abrahamsson,
1381 J., Kogner, P. and Martinsson, T. (2010) High-risk neuroblastoma tumors with 11q-
1382 deletion display a poor prognostic, chromosome instability phenotype with later
1383 onset. *Proc Natl Acad Sci U S A*, **107**, 4323-4328.
1384 73. Fransson, S., Ostensson, M., Djos, A., Javanmardi, N., Kogner, P. and Martinsson, T.
1385 (2016) Estimation of copy number aberrations: Comparison of exome sequencing data
1386 with SNP microarrays identifies homozygous deletions of 19q13.2 and CIC in
1387 neuroblastoma. *Int J Oncol*, **48**, 1103-1116.
1388 74. Kocak, H., Ackermann, S., Hero, B., Kahlert, Y., Oberthuer, A., Juraeva, D., Roels, F.,
1389 Theissen, J., Westermann, F., Deubzer, H. *et al.* (2013) Hox-C9 activates the intrinsic
1390 pathway of apoptosis and is associated with spontaneous regression in
1391 neuroblastoma. *Cell Death Dis*, **4**, e586.
1392 75. Cun, Y., Yang, T.P., Achter, V., Lang, U. and Peifer, M. (2018) Copy-number analysis and
1393 inference of subclonal populations in cancer genomes using Sclust. *Nat Protoc*, **13**,
1394 1488-1501.
1395 76. Zhang, W., Yu, Y., Hertwig, F., Thierry-Mieg, J., Zhang, W., Thierry-Mieg, D., Wang, J.,
1396 Furlanello, C., Devanarayan, V., Cheng, J. *et al.* (2015) Comparison of RNA-seq and
1397 microarray-based models for clinical endpoint prediction. *Genome Biol*, **16**, 133.
1398 77. Schneider, C.A., Rasband, W.S. and Eliceiri, K.W. (2012) NIH Image to ImageJ: 25 years
1399 of image analysis. *Nat Methods*, **9**, 671-675.
1400

1401 **Figure legends:**

1402 **Figure 1:** (**A**) m^6A RNA Immunoprecipitation (m^6A RIP) on RNA isolated from U-2 OS cells
1403 followed by slot blot, probed with DIG-labeled TERRA probe. RNase A was used as a control.
1404 m^6A RIP in fragmented and non-fragmented RNA (**B**) Schematic diagram describing key steps
1405 of m^6A RIP performed on either fragmented or non-fragmented RNA isolated from Control-sh
1406 or METTL3-KD U-2 OS cells. (**C**) (top panel) m^6A RIP followed with fragmented and non-
1407 fragmented RNA followed by slot blot with DIG-labeled TERRA repeat probe. (Middle panel)

1408 Quantification of the slot blot. Unpaired *t*-test was used, **** $p < 0.0001$. (Lower panel)
1409 Western blot showing METTL3-KD.
1410 Detection of UUAG tetramer in TERRA RNA by RNA-MS analysis (**D**) Schematic diagram
1411 describing key steps of TERRA pulldown and RNA-MS analysis (**E**) Slot blot showing the
1412 specificity of TERRA pulldown**.** Probe against Luciferase (negative pulldown) and RNase A
1413 was used as a control. (**F**) [**left panel**] Base peak chromatogram (BPC): first and second row
1414 show BPC of Standard UUAGp, isolated m/z 651.07 (doubly charged) and Standard
1415 UUm^{6}AGp, isolated m/z 658.08 (doubly charged) respectively. Third and fourth rows show
1416 the BPC of the TERRA pulldown sample, isolated m/z 651.07 (doubly charged) and isolated
1417 m/z 658.08 (doubly charged) respectively. [**Right panel**] MS2 spectrum: first and second rows
1418 show the MS2 spectrum of Standard UUAGp, isolated m/z 651.07, and Standard UUm^{6}AGp,
1419 isolated m/z 658.08 respectively with ions of mass difference 14 (methylation) starting from
1420 m/z 673 and up. Y-axis represents relative abundance in percentage. Third and fourth rows
1421 show the MS2 spectrum of the sample, isolated m/z 651.07 and isolated m/z 658.08
1422 respectively with ions of mass difference 14 (methylation) starting from m/z 673 and up. Y-
1423 axis represents absolute abundance.
1424 (**G**) Proximity ligation assay (PLA) in U-2 OS cells expressing TRF1-mCherry depicting the
1425 interaction of TRF2 with METTL3 (left) and METTL14 (right). TRF1-mCherry (Red), PLA
1426 foci (green) in the nucleus (marked by DAPI in blue). Box plot shows the number of co-
1427 localizations between TRF1-mCherry and PLA signal.
1428 (**H**) TERRA foci (green) in U-2 OS cells expressing TRF1-mCherry (red). Box plot shows the
1429 number of co-localizations between TRF1-mCherry and TERRA.
1430 (**I**) m^{6}A immunofluorescence (IF) (red) was performed in U-2 OS along with TERRA foci
1431 (green). Box plot shows the number of co-localizations between TERRA and m^{6}A.
1432 Scale bar is 10 μm.
1433
1434 **Figure 2:** (**A**) Flow chart depicting the major step of m^{6}A RIP-seq along with RNA-seq
1435 performed either on Illumina platform or on Oxford Nanopore Technologies (ONT), to
1436 generate short and long RNA-seq reads respectively. (**B**) Browser screenshot of 50 kb region
1437 around the telomere ends in T2T assembly, showing TERRA RNA expression (CPM) from
1438 two active chromosome ends (Chr12p, Chr20q) and one less active chromosome end (Chr3p)
1439 using ONT long read and Illumina short-read RNA-seq. RNA Pol II (purple) and CTCF (pink)
1440 enrichment at 50 kb region around the telomere ends from publicly available RNA Pol II and

1441 CTCF ChIP-seq data which were re-analyzed with T2T human genome assembly. CpG islands
1442 are marked with green bars and the telomeric repeats in this region are marked with black bars.
1443 (**C**) Heatmap summarizing RNA-seq and m^6A RIP-seq data. Chromosomes are sorted based
1444 on high (dark violet-pink) and low (light violet-pink) subtelomeric TERRA transcription. Black
1445 dots denote m^6A RIP-seq peaks and black diamonds denote the differential modified m^6A sites
1446 detected by xPore from ONT long reads at subtelomeres.
1447 (**D**) Genome browser screenshots showing IP/input ratio tracks for m^6A RIP (Control-sh and
1448 METTL3-KD) or IgG RIP (Control-sh) at two active chromosome ends (Chr12p, Chr20q) and
1449 one inactive chromosome end (Chr3p). Red bars mark m^6A RIP peaks identified using MACS
1450 (for short reads) or the differential m^6A sites identified using xPore (for long reads) for the
1451 samples as denoted.
1452 (**E**) The m^6A enrichment profiles across all subtelomeres in T2T assembly in Control-sh and
1453 METTL3-KD. The m^6A RIP/input signals were normalized to spike-in and to the mappability
1454 likelihood of each chromosome ends. Subtelomeres (high and low TERRA transcription) were
1455 classified according to the normalized median expression are shown. (**F**) Box plot of spike-in,
1456 mappability-normalized m^6A RIP/input enrichment profiles of all chromosome ends. Statistical
1457 significance was calculated using the Wilcoxon test, **** $p < 0.0001$.
1458
1459 **Figure 3:** (**A**) TERRA foci (green) in U-2 OS cells after siRNA mediated KD of METTL3.
1460 Box plot showing the number of TERRA foci per nucleus. Dunnett's multiple comparisons test
1461 was used, ** $p < 0.01$; **** $p < 0.0001$. (**B**) (top panel): Western blot showing METTL3 level
1462 in stable shRNA-depleted U-2 OS cells. (Middle panel) TERRA foci (green) in U-2 OS cells
1463 with stable KD of METTL3. (bottom panel): Box plot shows the number of TERRA foci per
1464 nucleus. Dunnett's multiple comparisons test was used, **** $p < 0.0001$.
1465 (**C**) Localization of the γ-H2AX (green) over telomere in Control-sh and METTL3-KD cells.
1466 Telomere is detected by TRF2 staining (red). Box plot shows the number of overlaps of TRF2
1467 and γ-H2AX. Dunnett's multiple comparisons test was used, **** $p < 0.0001$.
1468 (**D**) Localization of γ-H2AX (green) over telomere (marked by TRF2) in bleomycin-treated
1469 Control and METTL3-KD cells 4 h post-treatment and followed by 20 h of recovery without
1470 bleomycin. Box plot shows the number of overlaps of TRF2 and γ-H2AX. Unpaired *t*-test were
1471 used, * $p < 0.05$; ** $p < 0.01$. (**E**) m^6A IF (red) along with TERRA foci (green) was performed
1472 in U-2 OS cells 4 h post-treatment and followed by 20 h of recovery without bleomycin. Box

1473 plot shows the number of overlaps of TERRA and m^6A signal. Unpaired *t*-test was used, ** p
1474 < 0.01.
1475 (**F**) Cartoon demonstrating recruitment of dCasRx-FTO to target RNA. (**G**) m^6A RIP followed
1476 by TERRA slot blot on RNA isolated from U-2 OS cells expressing dCasRx-FTO with either
1477 non-target control (NTC) or TERRA guide RNA. IgG antibody was used as a negative control
1478 for the RIP experiment. Bar graph shows the quantification of slot blot. Unpaired *t*-test was
1479 used, **** $p < 0.0001$. (**H**) TERRA RNA-FISH detecting TERRA foci (green) was performed
1480 on U-2 OS cells expressing dCasRx-FTO with either NTC or TERRA guide RNA. Box plot
1481 shows the quantification of TERRA foci per nucleus. Unpaired *t*-test was used, **** $p <$
1482 0.0001. (**I**) TERRA foci (green) in U-2 OS cells treated with various METTL3 inhibitors for 6
1483 h. Box plot shows the quantification of TERRA foci per nucleus. Dunnett's multiple
1484 comparisons test was used, **** $p < 0.0001$. Scale bar is 10 μm.
1485
1486 **Figure 4:**
1487 (**A**) TERRA foci (green) in U-2 OS cells with siRNA mediated transient KD of m^6A reader
1488 proteins as denoted. Box plot shows the number of TERRA foci per nucleus. Dunnett's multiple
1489 comparisons test was used, ** $p < 0.01$; **** $p < 0.0001$.
1490 (**B**) hnRNPA2B1 RIP followed by TERRA slot blot demonstrates the interaction of
1491 hnRNPA2B1 with TERRA RNA. IgG and RNase A treatment were used as control.
1492 (**C**) Scheme and results of the re-RIP (hnRNPA2B1-m^6A) experiment in Control-sh or
1493 METTL3-KD U-2 OS cells. First RIP was performed with hnRNPA2B1/IgG antibody, the
1494 precipitated RNA was further subjected to RIP with m^6A antibody. Finally, the RNA after re-
1495 RIP was blotted and probed with the TERRA probe. RIP with IgG served as a negative control.
1496 Bar graph shows the quantification of the slot blot. Sidak's multiple comparisons test was used,
1497 ** $p < 0.01$; **** $p < 0.0001$.
1498 (**D**) IF showing recruitment of dCasRx-FTO at TERRA but not to NTC leads to reduced
1499 hnRNPA2B1(green) occupancy at telomeres (TRF2, red). Box plot shows the number of
1500 overlaps of the hnRNPA2B1 and TRF2. Unpaired *t*-test was used, *** $p < 0.001$. (**E**) γ-H2AX
1501 (green) accumulation at telomeres (TRF2, red) in U-2 OS cells with siRNA mediated KD of
1502 hnRNPA2B1. Box plot shows the number of overlaps of the γ-H2AX and TRF2. Dunnett's
1503 multiple comparisons test was used, * $p < 0.05$; ** $p < 0.01$.
1504 Scale bar is 10 μm.
1505

1506 **Figure 5:**

1507 (**A**) Schematic diagram describing the DRIP and DRImR method to purify R-Loop bound RNA
1508 and R-loop bound m^6A modified RNA respectively. (**B**) Blot on the left is from RNA purified
1509 in the DRIP experiment and the blot on the right is from the DRImR experiment performed on
1510 U-2 OS cells. Experiments performed with IgG antibody or nucleic acid pre-treated with RNase
1511 H served as a control. RNase A treatment was done to affirm the presence of only RNA in the
1512 final elution in the lanes indicated. Blots were probed with a DIG-labeled TERRA probe. (**C**)
1513 RNA enriched in R-Loops from Control-sh or METTL3-KD U-2 OS cells were isolated by the
1514 DRIP method followed by slot blot assay. Blot was probed with a DIG-labeled TERRA probe.
1515 DRIP performed with IgG antibody or pre-treatment with RNase H served as a control. RNase
1516 A treatment was done to affirm the presence of only RNA in the final elution. Bar graph shows
1517 the quantification of the blots. Unpaired *t*-test was used, **** $p < 0.0001$.

1518 (**D**) TERRA RNA-FISH detecting TERRA foci (green) in Control-sh or METTL3-KD U-2 OS
1519 cells that were transfected with either Control siRNA or siRNAs against RNase H. Box plot
1520 shows the quantification of TERRA foci per nucleus. Tukey's multiple comparisons test was
1521 used, **** $p < 0.0001$.

1522 R-loop PLA assay (**E**) PLA in U-2 OS TRF1-mCherry cells with overexpression of either
1523 RNase H^{WT} (left) or RNase H^{Mut} (right) depicting the interaction of TRF2 with R-Loop (S9.6
1524 antibody). TRF1-mCherry (Red), PLA foci (green) in the nucleus (marked by DAPI). Box plot
1525 shows the number of overlaps of PLA signal and TRF1-mCherry per nucleus. Unpaired *t*-test
1526 was used, **** $p < 0.0001$. (**F, G**) PLA depicting the interaction of TRF2 with R-Loop (S9.6
1527 antibody) in U-2 OS TRF1-mCherry cells with (**F**) Control-sh or METTL3-KD (**G**) Control
1528 siRNA or hnRNPA2B1 siRNA2. TRF1-mCherry (Red), PLA foci (green) in the nucleus
1529 (marked by DAPI). Box plot shows the number of overlaps of PLA signal and TRF1-mCherry
1530 per nucleus. Unpaired *t*-test was used, **** $p < 0.0001$.

1531 Scale bar is 10 μm.

1532

1533 **Figure 6:** (**A**) Profiling TERRA RNA expression in ALT+/- cell lines by slot blot assay
1534 performed with 100, 200 and 400 ng of RNA isolated from cell lines indicated. Blot probed
1535 with a DIG-labeled TERRA probe. TapeStation profile on the right shows 18s and 28s rRNA
1536 served as a loading control. Bar graph shows the TERRA level quantified from blots and
1537 normalized to loading control.

1538 (**B**) m^6A RIP followed by TERRA slot blot on RNA isolated from SK-N-F1 (ALT+), SK-N-
1539 BE(2), and IMR-32 (ALT-) cell lines. RIP with IgG severed as a negative control. Bar graph

1540 shows the quantification of the blots. Sidak's multiple comparisons test was used, **** $p <$
1541 0.0001.
1542 (**C**) TERRA RNA foci (green) visualized by TERRA RNA-FISH in ALT+ (upper panel) and
1543 ALT- (lower panel) NB cell lines. Box plot shows the quantification of the TERRA foci per
1544 nucleus.
1545 (**D**) TERRA foci (green) combined with m^6A (red) IF in CHLA-90 (left) and SK-N-F1 (right)
1546 cells. Box plot shows the number of overlaps of TERRA and m^6A per nucleus. Scale bar is 10
1547 μm.
1548 (**E**) The m^6A enrichment profiles across all subtelomeres using T2T assembly in SK-N-F1 and
1549 SK-N-BE(2) cells. The m^6A RIP/input signals were normalized to spike-in and to the
1550 mappability likelihood of each chromosome ends. (**F**) Box plot of spike-in, mappability-
1551 normalized m^6A RIP/input enrichment profiles of all subtelomeres in SK-N-F1 and SK-N-
1552 BE(2). Statistical significance was calculated using the Wilcoxon test, **** $p < 0.0001$.
1553 (**G**) TERRA RNA expression in ALT+/- NB patient tumor samples were detected by slot blot
1554 assay performed with 100 ng of RNA. The tumor profile indicates genomic alteration. These
1555 tumors were also assayed for C-Circle (CCA).
1556 (**H**) Representative browser screenshot of 50 kb region around the telomere ends, showing
1557 TERRA RNA expression (CPM) from two of the active chromosome ends (Chr9p, Chr16q)
1558 and one inactive chromosome end (Chr3p) using Illumina short read RNA-seq performed on
1559 NB1 and NB2 tumor samples. CpG islands are marked with green bars and the telomeric
1560 repeats in this region are marked with black bars.
1561 (**I**) Heatmap summarizing RNA-seq and m^6A RIP-seq data of two NB tumor samples (NB1
1562 and NB2). Chromosomes are sorted based on high (dark colored) and low (light colored)
1563 subtelomeric TERRA transcription. Black dots denote m^6A RIP-seq peaks identified using
1564 MACS peak caller in these NB tumor samples.
1565 (**J**) Genome browser screenshots showing m^6A RIP/input ratio tracks for NB1 and NB2 tumor
1566 samples at two active chromosome ends (Chr12p, Chr20q) and one inactive chromosome end
1567 (Chr3p). Red bars mark m^6A RIP peaks identified using MACS peak caller.
1568 (**K**) The m^6A enrichment profiles across subtelomeres using T2T assembly in NB1 and NB2
1569 tumors. The m^6A RIP/input signals were normalized to spike-in and to the mappability
1570 likelihood of each chromosome ends. Subtelomeres (high and low TERRA transcription) were
1571 classified according to the normalized median expression are shown.
1572 (**L**) Event-free survival of NB patients (n=498, SEQC cohort) with either low (blue) or high
1573 (red) expression of METTL3.

1574 (**M**) Event-free survival of ALT+ NB patients (n=21) with either low (blue) or high (red)
1575 expression of METTL3.
1576 (**N**) Bar graph showing percentage of ALT+ or MNA (MYCN amplified) tumors with copy
1577 number gain in METTL3, METTL14, or hnRNPA2B1 genes.
1578
1579 **Figure 7:** TERRA foci following siRNA mediated METTL3 depletion in ALT+ NB cells (**A**)
1580 (left panel) Western blot for METTL3 level after siRNA transfection in CHLA-90 cells.
1581 (middle panel) TERRA RNA-FISH detecting TERRA foci (green) in CHLA-90 and SK-N-F1
1582 cells after METTL3 knockdown as indicated. (right panel) Box plots show the quantification
1583 of TERRA foci per nucleus. Dunnett's multiple comparisons test was used, * $p < 0.05$; ** $p <$
1584 0.01; **** $p < 0.0001$.
1585 (**B**) Representative images from colony formation assay performed on CHLA-90 (top) and SK-
1586 N-F1(bottom) cells with TetO Control or METTL3-KD.
1587 (**C**) TERRA RNA FISH in TetO Control and METTL3-KD SK-N-F1 and CHLA-90 cells. Box
1588 plot shows the quantification of the TERRA foci in the indicated conditions. Unpaired *t*-test
1589 was used, *** $p < 0.001$.
1590 (**D**) Accumulation of γ-H2AX (red) over telomere after 48 h of Dox induction in SK-N-F1
1591 TetO METTL3-KD cells. Telomeres were detected by telomere DNA FISH (green). Box plot
1592 shows the overlap of telomere and γ-H2AX. Unpaired *t*-test was used, **** $p < 0.0001$.
1593 (**E**) (top panel) Line graph showing average tumor growth (mm^3) of SK-N-F1 cells (TetO
1594 Control and METTL3-KD) derived xenografts over time. Data are shown as Mean ± SD.
1595 Sidak's multiple comparisons test was used, **** $p < 0.0001$. (bottom panel) plot showing
1596 tumor weight post necropsies of xenografts derived from SK-N-F1 cells with either TetO
1597 Control or METTL3-KD. Data are shown as Mean ± SD. Unpaired *t*-test was used, * $p < 0.05$
1598 (n=4). One representative image of the tumor is shown per condition.
1599 (**F**) Western blot to verify the hnRNPA2B1 KD in ALT+ NB cells. Vinculin was used as a
1600 loading control. (**G**) TERRA foci (green) in CHLA-90 (top) and SK-N-F1 (bottom) cells after
1601 transient KD of hnRNPA2B1. Box plot shows the quantification of TERRA foci per nucleus.
1602 Unpaired *t*-test was used, ** $p < 0.01$; **** $p < 0.0001$.
1603 (**H**) TERRA RNA-FISH detecting TERRA foci (green) in CHLA-90 (top panel) and SK-N-F1
1604 (bottom panel) cells treated with METTL3 inhibitors (10 μM STM2457, 50 μM UZH1A, and
1605 50 μM UZH1B) for 6 h. DMSO treatment served as a control. Box plot showing quantification

1606 of the TERRA foci as indicated. Dunnett's multiple comparisons test was used, * $p < 0.05$; ***
1607 $p < 0.001$; **** $p < 0.0001$.
1608 (**I**) Telomere DNA FISH (green) and γ-H2AX IF (red) in SK-N-F1 cells treated with METTL3
1609 inhibitor, STM2457 for 48 h. Box plot showing quantification of telomere and γ-H2AX
1610 overlap. Unpaired *t*-test was used, **** $p < 0.0001$. Scale bar is 10 μm.
1611 (**J**) Cell viability was measured by MTT assay after treating CHLA-90 and SK-N-F1 cells with
1612 10 μM of METTL3 inhibitor (STM2457) at indicated time points. Data are normalized to
1613 DMSO control. Sidak's multiple comparisons test was used, **** $p < 0.0001$.
1614
1615 **Supplementary Figure legends:**
1616 **Supplementary Figure S1:**
1617 (**A**) TapeStation profile of RNA isolated from Control-sh or METTL3-KD U-2 OS cells which
1618 is either fragmented or non-fragmented. Serving as a control for Figure 1C.
1619 (**B**) Schematic diagram shows *In vitro* METTL3/METTL14 methyltransferase assay performed
1620 with DRACH oligo or TERRA repeat containing oligo. A and m^6A were detected and
1621 quantified by LC-MS/MS-based method. RNA oligo Standard with or without m^6A was used
1622 as a control. Bar graph shows the ratio of A/m^6A in the indicated conditions. Unpaired *t*-tests
1623 were used, * $p < 0.05$; **** $p < 0.0001$.
1624 (**C**) Background control for PLA with only TRF2 and only METTL3 in U-2 OS cells
1625 expressing TRF1-mCherry in the nucleus (marked by DAPI).
1626 (**D**) Chromatin Immunoprecipitation (ChIP) using METTL3 antibody on U-2 OS cells
1627 followed by slot blot. Blot probed with a DIG-labeled TERRA probe. IgG antibody was used
1628 as a negative control.
1629 (**E**) TERRA foci (green) in U-2 OS cells treated with either Scrambled or TERRA LNA. Box
1630 plot shows the quantification of TERRA signal per nucleus. Unpaired *t*-test was used, ** $p <$
1631 0.01.
1632 Scale bar is 10 μm.
1633
1634 **Supplementary Figure S2:**
1635 (**A**) Genome browser tracks of normalized CPM coverage obtained from Strand-specific
1636 Illumina short-reads in U-2 OS cells showing transcription away from telomere ends (direction
1637 of transcription is opposite to TERRA). Reads were mapped to the positive strand on p arms,

1638 and the negative strand on q arms, to match the direction of transcription, are shown for two
1639 active chromosome ends (Chr12p, Chr20q) and one inactive chromosome end (Chr3p).
1640 (**B-C**) Characterizing the high and low TERRA RNA expressing subtelomeres using
1641 normalized read counts from either (**B**) Illumina short reads or (**C**) ONT-long reads. Read
1642 counts were normalized using CPM and to the mappability likelihood of each chromosome
1643 ends. Statistical significance was calculated using the two-sided paired *t*-test.
1644 (**D**) Slot blot with total RNA isolated from Control-sh or METTL3-KD U-2 OS cells. Blot
1645 probed with a DIG-labeled TERRA probe. TapeStation profile showing 18s and 28s rRNA
1646 served as a loading control. Bar graph shows the quantification of the blot normalized to the
1647 respective loading control. Unpaired *t*-test was used, ** $p < 0.01$.
1648 (**E**) Metagene plot showing density distribution of m^6A peak or m^6A sites per bin from both
1649 m^6A RIP peaks (red) and m^6A xPore sites (blue). (**F**) Identified top enriched motif logo from
1650 de novo motif analysis of m^6A peaks from m^6A RIP-seq and m^6A xPore sites. (**G**) Bar plot
1651 summarizing peaks identified genome-wide in RIP-seq experiment. (**H**) Telomeric repeat
1652 reads enriched in m^6A/IgG RIP-seq using TelomereHunter.
1653 (**I**) Venn diagram showing the overlap between m^6A RIP peaks (red) and m^6A xPore sites
1654 (blue) at the 3' UTR.
1655 (**J**) Enrichment of m^6A RIP/input signal at DRACH motif coordinates located within the
1656 subtelomeric m^6A RIP-seq peaks in Control-sh and METTL3-KD U-2 OS cells. Statistical
1657 significance was calculated using the two-sided paired *t*-test. ****: $p < 0.0001$.
1658 (**K**) Scatter plot depicting differentially modified sites identified using xPore from Control-sh
1659 and METTL3-KD U-2 OS long-reads. Predicted modified k-mers within the 30 kb
1660 subtelomeres regions showing a positive modification rate in Control-sh within the NNANN
1661 context being differentially modified as compared to METTL3-KD are shown.
1662
1663 **Supplementary Figure S3:**
1664 (**A**) IF showing METTL3-KD following METTL3 siRNA treatment. Bar graph shows the
1665 quantification of the images as indicated. Dunnett's multiple comparisons test was used, ** p
1666 < 0.01. (**B**) (left panel) Western blot to verify METTL14 siRNA mediated knockdown in U-2
1667 OS cells. Vinculin was used as a loading control. (middle panel) TERRA foci (green) in U-2
1668 OS cells within Control or METTL14 siRNA treated cells. Nucleus marked by DAPI. (right
1669 panel) Box plot shows TERRA signal per nucleus in the condition indicated. Dunnett's multiple
1670 comparisons test was used, *** $p < 0.001$; **** $p < 0.0001$.

1671 (**C**) Localization of the γ-H2AX (green) over telomere in Scrambled or TERRA LNA cells.
1672 Telomere is detected by TRF2 staining (red). Box plot shows the overlap of TRF2 and γ-H2AX.
1673 Unpaired *t*-test was used, **** $p < 0.0001$.
1674 (**D**) IF of TRF2 (red) and PML bodies (green) in control and METTL3-KD U-2 OS cells. Box
1675 plot shows the overlap of PML and TRF2. Dunnett's multiple comparisons test was used, * p
1676 < 0.05. Scale bar is 10 µm.
1677 (**E**) (Top panel) Slot blot with total RNA isolated from U-2 OS cells expressing dCasRx-FTO
1678 with either NTC or TERRA guide RNA. RNA was loaded in 3 different amounts100, 200, and
1679 400 ng. Blot probed with a DIG-labeled TERRA probe. TapeStation profile showing 18s and
1680 28s rRNA served as a loading control. Bar graph shows the quantification of the blot
1681 normalized to loading control. Unpaired *t*-test was used. (Bottom panel) Western blot to verify
1682 induction of HA-tagged dCasRx-FTO by Dox. GAPDH is loading control.
1683 (**F**) (Top panel) Slot blot with total RNA isolated from U-2 OS cells expressing catalytically
1684 active CasRx-HA with either NTC or TERRA guide RNA. RNA was loaded in 2 different
1685 amounts100 ng and 200 ng. Blot probed with DIG-labeled TERRA repeat-containing probe.
1686 TapeStation profile showing 18s and 28s rRNA served as a loading control. Bar graph shows
1687 the quantification of the blot normalized to loading control. Unpaired *t*-test was used, *** $p <$
1688 0.001. (Bottom panel) Western blot to verify induction of CasRx-HA by Dox. GAPDH is
1689 loading control.
1690 (**G**) TERRA slot blot with total RNA isolated from U-2 OS cells treated with Actinomycin D
1691 for the indicated time points.
1692 (**H**) TERRA slot blot with total RNA isolated from U-2 OS cells treated with METTL3
1693 inhibitor, STM2457. DMSO served as a control for STM2457. TapeStation profile showing
1694 18s and 28s rRNA served as a loading control. Bar graph shows the quantification of the blot
1695 normalized to loading control. Unpaired *t*-test was used.
1696
1697 **Supplementary Figure S4:**
1698 (**A**) Relative mRNA expression of m^6A reader proteins- hnRNPA2B1, YTHDC1, RBMX, and
1699 YTHDF2 that were knocked down with siRNA. GAPDH was used to normalize the qPCR data.
1700 Dunnett's multiple comparisons test was used, ** $p < 0.01$; **** $p < 0.0001$.
1701 (**B**) Slot blot with total RNA isolated from U-2 OS cells with either control or hnRNPA2B1
1702 siRNA. RNA was loaded in 2 different amounts 100 and 200 ng. Blot probed with a DIG-
1703 labeled TERRA probe. TapeStation profile showing 18s and 28s rRNA served as a loading

1704 control. Bar graph shows the quantification of the blot normalized to loading control. Unpaired
1705 *t*-test was used.
1706 (**C**) *In vitro* binding assay between total RNA isolated from Control-sh or METTL3-KD U-2
1707 OS cells (2 different RNA concentrations) with purified His-tagged hnRNPA2B1. Left panel
1708 show commissive staining of purified hnRNPA2B1 bound to beads. Right panel, hnRNPA2B1
1709 bound RNA fraction on slot blot probed with DIG-labeled TERRA probe. Bar graph shows the
1710 quantification of the blots. Unpaired *t*-test was used, ** $p < 0.01$.
1711
1712 **Supplementary Figure S5:**
1713 (**A**) TERRA RNA-FISH detecting TERRA foci (green) in U-2 OS cells exogenously treated
1714 with either mock, RNase A, RNase H, or with both RNase A and RNase H. Box plot shows the
1715 number of TERRA foci per nucleus. Dunnett's multiple comparisons test was used, **** $p <$
1716 0.0001.
1717 (**B**) Relative RNase H expression following siRNA mediated KD. GAPDH was used to
1718 normalize the qPCR data. Dunnett's multiple comparisons test was used, **** $p < 0.0001$.
1719 (**C**) Nucleic acid isolated from U-2 OS cells overexpressing RNase H^{WT} or RNase H^{Mut} were
1720 immobilized onto a nitrocellulose membrane and immunoblotted with S9.6 antibody. Bar
1721 graph is the quantification of the blot. Unpaired *t*-test was used, **** $p < 0.0001$.
1722 (**D**) TERRA foci (green) in U-2 OS cells overexpressing RNase H^{WT} (left) or RNase H^{Mut}
1723 (right). Box plot shows the quantification of the TERRA foci per nucleus. Unpaired *t*-test was
1724 used, **** $p < 0.0001$.
1725 (**E**) Background control for PLA with only TRF2 (left); or only S9.6 (right) antibody in RNase
1726 H^{Mut} U-2 OS cells expressing TRF1-mCherry.
1727 (**F**) PLA depicting the interaction of TRF2 with R-loop (S9.6 antibody) in U-2 OS TRF1-
1728 mCherry cells expressing dCasRx-FTO with either NTC (left) or TERRA guide RNA (right).
1729 Box plot shows the quantification of the overlapping PLA and TRF1-mCherry signal. Unpaired
1730 *t*-test was used, ** $p < 0.01$. Scale bar is 10 μm.
1731
1732 **Supplementary Figure S6:**
1733 (**A**) C-Circle assay (CCA) was performed on DNA from ALT+ and ALT- NB cells. Bar graph
1734 shows the quantification of the blots.
1735 (**B**) TERRA foci (green) in ALT+ CHLA-90 (top) and SK-N-F1 (bottom) cells treated with
1736 either Scrambled or TERRA LNA. Scale bar is 10 μm.

1737 (**C**) Subtelomeric TERRA expression (CPM) in SK-N-F1 and SK-N-BE(2) cells using
1738 mappability normalized RNA-seq data. Statistical significance was calculated using the two-
1739 sided paired *t*-test, **** $p < 0.0001$.
1740 (**D**) Top enriched motif logo from de novo motif analysis of m^6A peaks from SK-N-F1 and
1741 SK-N-BE(2) m^6A RIP-seq data.
1742 (**E**) C-Circle assay (CCA) was performed on DNA from NB tumors.
1743 (**F**) Subtelomeres are characterized as high and low on TERRA expression (CPM) in NB1 and
1744 NB2 tumors using mappability normalized RNA-seq data. Statistical significance was
1745 calculated using the two-sided paired *t*-test, *** $p < 0.001$.
1746 (**G**) Top enriched motif logo from de novo motif analysis of NB1 and NB2 tumor m^6A peaks.
1747 (**H**) Event-free survival of NB patients (n=498, SEQC cohort) with either low (blue) or high
1748 (red) expression of METTL14 and hnRNPA2B1.
1749 (**I**) Event-free survival of ALT+ NB patients (n=21) with either low (blue) or high (red)
1750 expression of METTL14 and hnRNPA2B1.
1751
1752 **Supplementary Figure S7:**
1753 (A)Western blot showing METTL3 level in TetO Control and METTL3-KD ALT+ NB cells
1754 following Dox induction for 48 h. GAPDH was loading control. (**B**) Bar graph displaying the
1755 effect on cell viability after conditional KD of METTL3 (6 days post Dox treatment) in CHLA-
1756 90 and SK-N-F1 TetO METTL3-KD cells. Data normalized to control and shown as Mean ±
1757 SD. Unpaired *t*-test was used, **** $p < 0.0001$.
1758 (**C**) Slot blot with total RNA isolated from SK-N-F1 cells with TetO Control or METTL3-KD.
1759 RNA was loaded in 2 different amounts 200 and 400 ng. Blot probed with a DIG-labeled
1760 TERRA probe. TapeStation profile showing 18s and 28s RNA served as a loading control. Bar
1761 graph showing quantification normalized to loading control. Unpaired *t*-test was used.
1762 (**D**) Accumulation of γ-H2AX (red) over telomere after 48 h of Dox induction in CHLA-90
1763 cells with TetO METTL3-KD. Telomere was detected by telomere DNA FISH (green). Box
1764 plot shows the quantification of γ-H2AX, and telomere overlap. Unpaired *t*-test was used, ****
1765 $p < 0.0001$.
1766 (**E**) C-circle assay results visualized on a slot blot. DNA isolated from CHLA-90 and SK-N-
1767 F1 cells with TetO METTL3-KD (48 h Dox treatment) was subjected to a C-circle assay
1768 with/without Phi29 polymerase (Pol+/Pol-). Bar graph shows the quantification of the blots.
1769 Sídak's multiple comparisons test was used, ** $p < 0.01$; *** $p < 0.001$.

1770

1771 (**F**) DRIP followed by slot blot assay and probed with DIG-labeled TERRA probe in TetO
1772 Control or METTL3-KD SK-N-F1 cells, 72 h post-Dox induction. Experiments performed
1773 with IgG antibody or nuclei acid pre-treated with RNase H served as a control.
1774 (**G**) (Left panel) Line graph showing average tumor growth (mm^3) of CHLA-90 cells (TetO
1775 Control and METTL3-KD) derived xenografts over time. Data are shown as Mean ± SD.
1776 Sidak's multiple comparisons test was used, **** $p < 0.0001$. (Middle panel) Tumor weight
1777 post necropsies of xenografts derived from CHLA-90 cells with either TetO Control or
1778 METTL3-KD Data are shown as Mean ± SD. Unpaired *t*-test was used, ** $p < 0.01$ (n=3). One
1779 representative image of the tumor is shown per condition. (Right panel) Western blot confirms
1780 the METTL3-KD in xenograft tumors and GAPDH acted as a loading control.
1781 (**H**) TERRA RNA-FISH detecting TERRA foci (green) combined with hnRNPA2B1 (red) IF
1782 in CHLA-90 cells. Box plot shows the quantification of TERRA and m^6A overlap.
1783 (**I**) Telomere DNA FISH (green) and γ-H2AX IF (red) in ALT- SK-N-BE(2) cells treated with
1784 METTL3 inhibitor, STM2457 for 48 h. Box plot showing quantification of telomere and γ-
1785 H2AX overlap. Unpaired *t*-test was used. Scale bar is 10 μm.

Figure 1

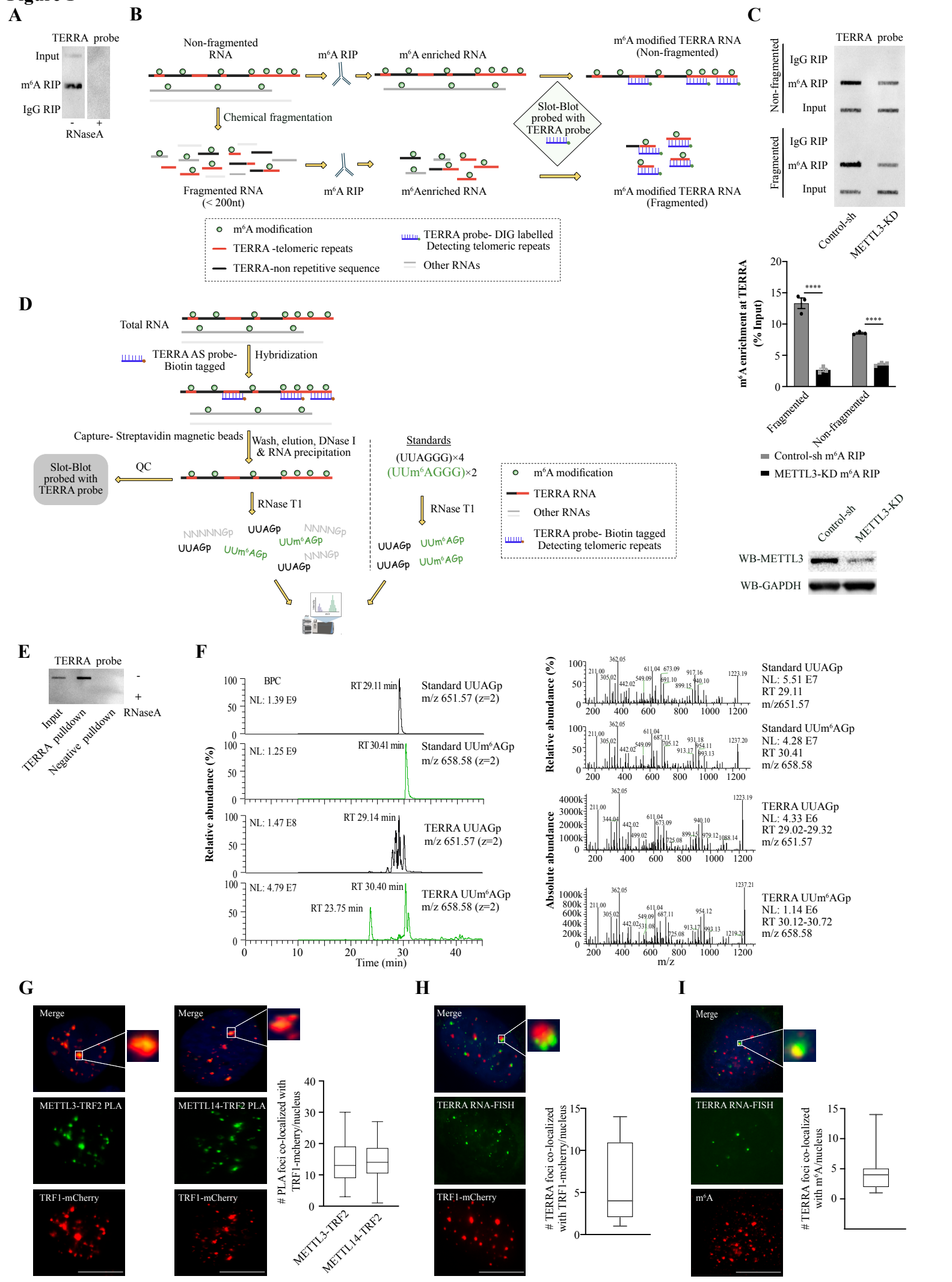
A
TERRA probe
Input
m6A RIP
IgG RIP
-
+
RNaseA
B
Non-fragmented RNA
m6A RIP
m6A enriched RNA
Chemical fragmentation
Fragmented RNA (< 200nt)
m6A RIP
m6Aenriched RNA
Slot-Blot probed with TERRA probe
m6A modified TERRA RNA (Non-fragmented)
m6A modified TERRA RNA (Fragmented)
m6A modification
TERRA -telomeric repeats
TERRA-non repetitive sequence
TERRA probe- DIG labelled Detecting telomeric repeats
Other RNAs
C
TERRA probe
Non-fragmented
IgG RIP
m6A RIP
Input
Fragmented
IgG RIP
m6A RIP
Input
Control-sh
METTL3-KD
m6A enrichment at TERRA (% Input)
****
****
Fragmented
Non-fragmented
Control-sh m6A RIP
METTL3-KD m6A RIP
Control-sh
METTL3-KD
WB-METTL3
WB-GAPDH
D
Total RNA
TERRA AS probe- Biotin tagged
Hybridization
Capture- Streptavidin magnetic beads
Wash, elution, DNase I & RNA precipitation
QC
Slot-Blot probed with TERRA probe
RNase T1
NNNNNGp
UUAGp
UUm6AGp
NNNGp
Standards
(UUAGGG)×4
(UUm6AGGG)×2
m6A modification
TERRA RNA
Other RNAs
TERRA probe- Biotin tagged Detecting telomeric repeats
E
TERRA probe
Input
TERRA pulldown
Negative pulldown
-
+
RNaseA
F
BPC
NL: 1.39 E9
RT 29.11 min
Standard UUAGp m/z 651.57 (z=2)
NL: 1.25 E9
RT 30.41 min
Standard UUm6AGp m/z 658.58 (z=2)
NL: 1.47 E8
RT 29.14 min
TERRA UUAGp m/z 651.57 (z=2)
NL: 4.79 E7
RT 30.40 min
RT 23.75 min
TERRA UUm6AGp m/z 658.58 (z=2)
Relative abundance (%)
Time (min)
Standard UUAGp NL: 5.51 E7 RT 29.11 m/z651.57
Standard UUm6AGp NL: 4.28 E7 RT 30.41 m/z 658.58
TERRA UUAGp NL: 4.33 E6 RT 29.02-29.32 m/z 651.57
TERRA UUm6AGp NL: 1.14 E6 RT 30.12-30.72 m/z 658.58
Absolute abundance
m/z
G
Merge
METTL3-TRF2 PLA
TRF1-mCherry
METTL14-TRF2 PLA
PLA foci co-localized with TRF1-mcherry/nucleus
METTL3-TRF2
METTL14-TRF2
H
TERRA RNA-FISH
TERRA foci co-localized with TRF1-mcherry/nucleus
I
m6A
TERRA foci co-localized with m6A/nucleus

Figure 2

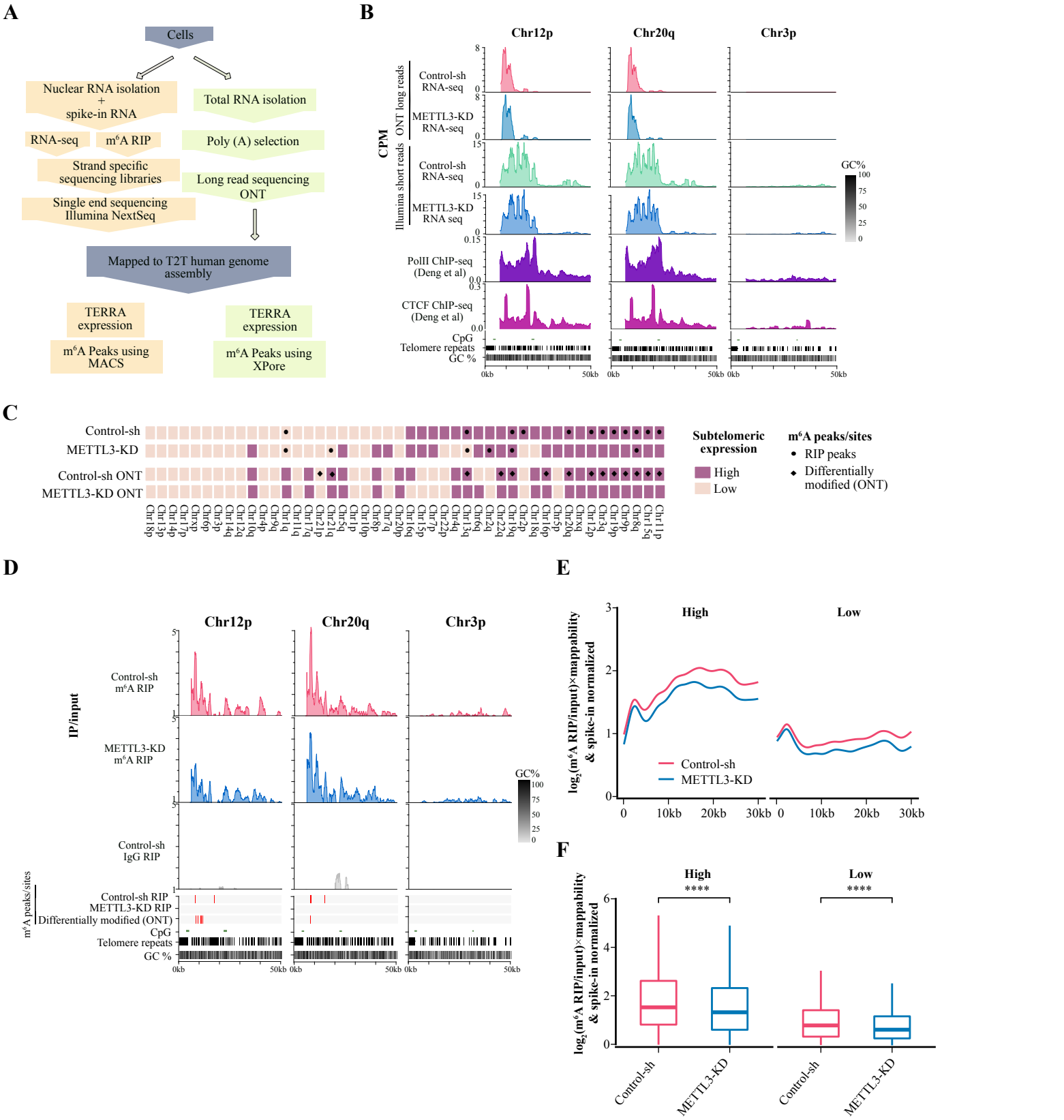
A
Cells
Nuclear RNA isolation + spike-in RNA
Total RNA isolation
RNA-seq
m6A RIP
Poly (A) selection
Strand specific sequencing libraries
Long read sequencing ONT
Single end sequencing Illumina NextSeq
Mapped to T2T human genome assembly
TERRA expression
TERRA expression
m6A Peaks using MACS
m6A Peaks using XPore
B
Chr12p
Chr20q
Chr3p
CPM
ONT long reads
Illumina short reads
Control-sh RNA-seq
METTL3-KD RNA-seq
Control-sh RNA-seq
METTL3-KD RNA seq
PolII ChIP-seq (Deng et al)
CTCF ChIP-seq (Deng et al)
CpG
Telomere repeats
GC %
GC%
0kb
50kb
C
Control-sh
METTL3-KD
Control-sh ONT
METTL3-KD ONT
Subtelomeric expression
High
Low
m6A peaks/sites
RIP peaks
Differentially modified (ONT)
D
Chr12p
Chr20q
Chr3p
IP/input
Control-sh m6A RIP
METTL3-KD m6A RIP
Control-sh IgG RIP
m6A peaks/sites
Control-sh RIP
METTL3-KD RIP
Differentially modified (ONT)
CpG
Telomere repeats
GC %
GC%
0kb
50kb
E
High
Low
log2(m6A RIP/input)×mappability & spike-in normalized
Control-sh
METTL3-KD
0
10kb
20kb
30kb
F
High
Low
****
****
log2(m6A RIP/input)×mappability & spike-in normalized
Control-sh
METTL3-KD
Control-sh
METTL3-KD

Figure 3

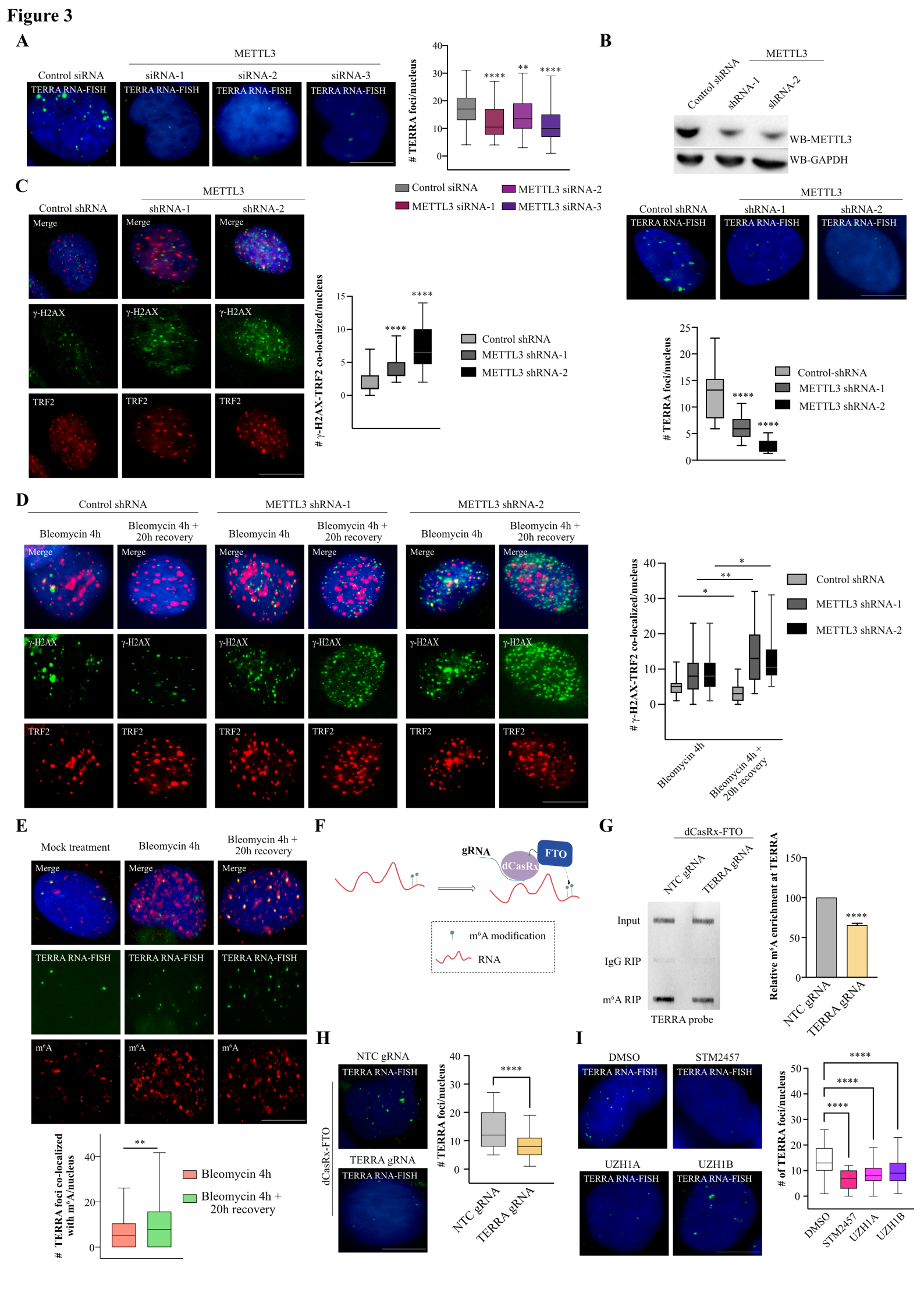
A
METTL3
Control siRNA
siRNA-1
siRNA-2
siRNA-3
TERRA RNA-FISH
TERRA foci/nucleus
****
**
****
B
METTL3
Control shRNA
shRNA-1
shRNA-2
WB-METTL3
WB-GAPDH
C
METTL3
Control shRNA
shRNA-1
shRNA-2
Merge
γ-H2AX
TRF2
γ-H2AX-TRF2 co-localized/nucleus
Control siRNA
METTL3 siRNA-1
METTL3 siRNA-2
METTL3 siRNA-3
Control shRNA
METTL3 shRNA-1
METTL3 shRNA-2
TERRA RNA-FISH
TERRA foci/nucleus
Control-shRNA
METTL3 shRNA-1
METTL3 shRNA-2
D
Control shRNA
METTL3 shRNA-1
METTL3 shRNA-2
Bleomycin 4h
Bleomycin 4h + 20h recovery
Merge
γ-H2AX
TRF2
γ-H2AX-TRF2 co-localized/nucleus
Control shRNA
METTL3 shRNA-1
METTL3 shRNA-2
E
Mock treatment
Bleomycin 4h
Bleomycin 4h + 20h recovery
Merge
TERRA RNA-FISH
m6A
TERRA foci co-localized with m6A/nucleus
Bleomycin 4h
Bleomycin 4h + 20h recovery
F
gRNA
dCasRx
FTO
m6A modification
RNA
G
dCasRx-FTO
NTC gRNA
TERRA gRNA
Input
IgG RIP
m6A RIP
TERRA probe
Relative m6A enrichment at TERRA
H
NTC gRNA
TERRA gRNA
dCasRx-FTO
TERRA RNA-FISH
TERRA foci/nucleus
I
DMSO
STM2457
UZH1A
UZH1B
TERRA RNA-FISH
# of TERRA foci/nucleus

Figure 4

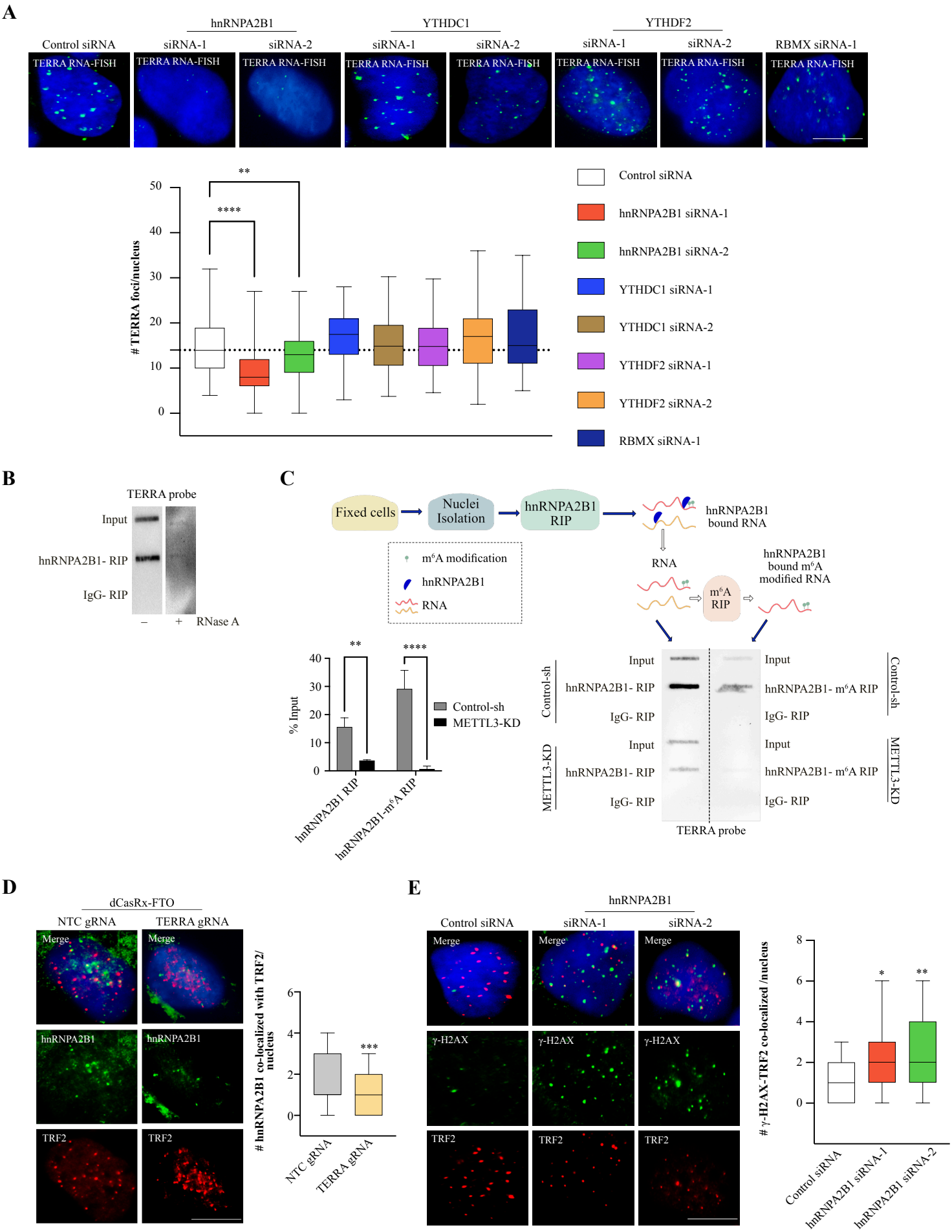
A
hnRNPA2B1
YTHDC1
YTHDF2
Control siRNA
siRNA-1
siRNA-2
siRNA-1
siRNA-2
siRNA-1
siRNA-2
RBMX siRNA-1
TERRA RNA-FISH
TERRA foci/nucleus
Control siRNA
hnRNPA2B1 siRNA-1
hnRNPA2B1 siRNA-2
YTHDC1 siRNA-1
YTHDC1 siRNA-2
YTHDF2 siRNA-1
YTHDF2 siRNA-2
RBMX siRNA-1
B
TERRA probe
Input
hnRNPA2B1- RIP
IgG- RIP
RNase A
C
Fixed cells
Nuclei Isolation
hnRNPA2B1 RIP
hnRNPA2B1 bound RNA
m6A modification
hnRNPA2B1
RNA
m6A RIP
hnRNPA2B1 bound m6A modified RNA
% Input
Control-sh
METTL3-KD
hnRNPA2B1 RIP
hnRNPA2B1-m6A RIP
hnRNPA2B1- m6A RIP
TERRA probe
D
dCasRx-FTO
NTC gRNA
TERRA gRNA
Merge
hnRNPA2B1
TRF2
hnRNPA2B1 co-localized with TRF2/ nucleus
E
hnRNPA2B1
Control siRNA
siRNA-1
siRNA-2
γ-H2AX
γ-H2AX-TRF2 co-localized /nucleus

Figure 5

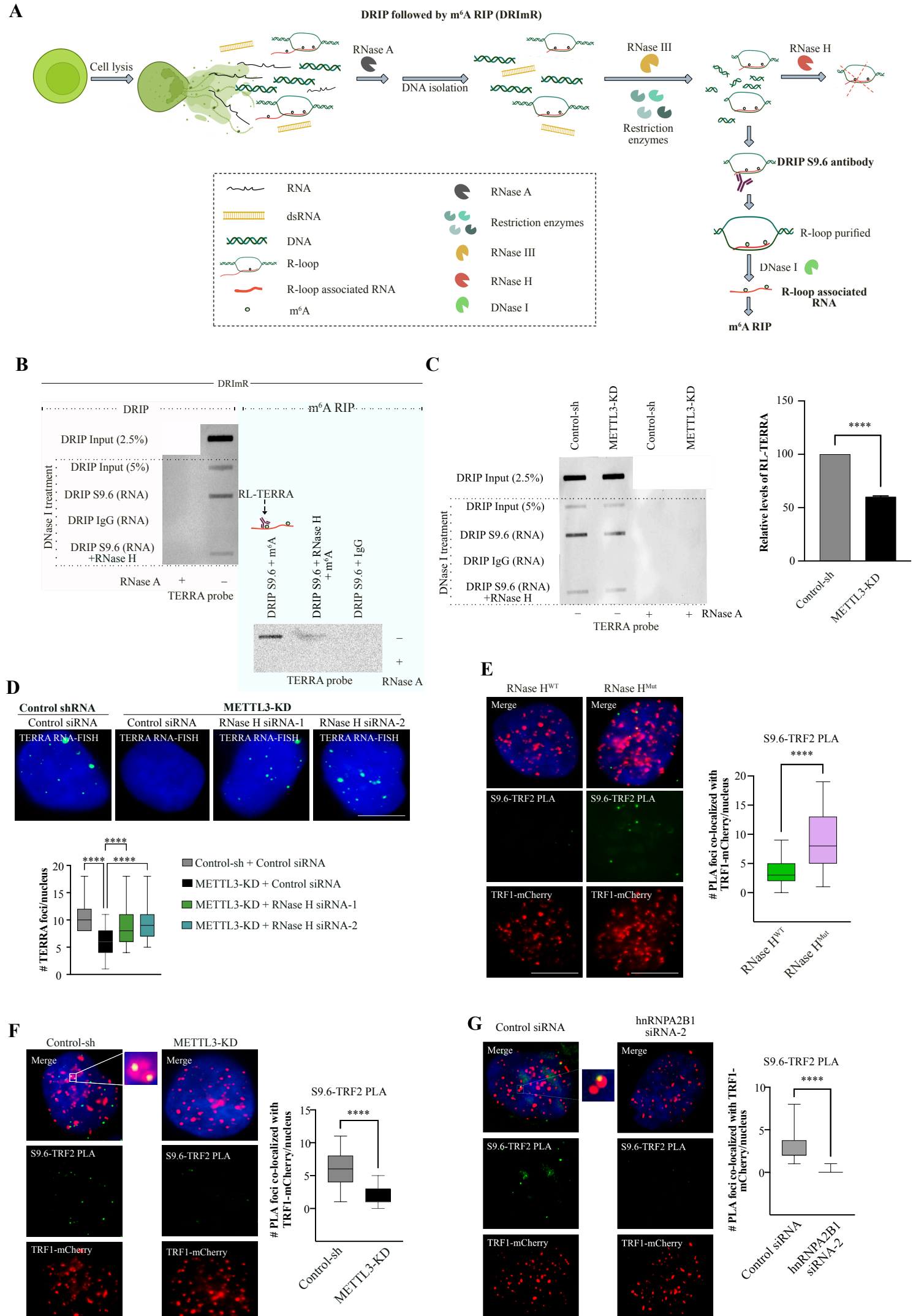
A
DRIP followed by m6A RIP (DRImR)
Cell lysis
RNase A
DNA isolation
RNase III
Restriction enzymes
RNase H
DRIP S9.6 antibody
R-loop purified
DNase I
R-loop associated RNA
m6A RIP
RNA
dsRNA
DNA
R-loop
R-loop associated RNA
m6A
RNase A
Restriction enzymes
RNase III
RNase H
DNase I
B
DRImR
DRIP
m6A RIP
DRIP Input (2.5%)
DRIP Input (5%)
DRIP S9.6 (RNA)
DRIP IgG (RNA)
DRIP S9.6 (RNA) +RNase H
DNase I treatment
RL-TERRA
RNase A
TERRA probe
DRIP S9.6 + m6A
DRIP S9.6 + RNase H + m6A
DRIP S9.6 + IgG
C
Control-sh
METTL3-KD
Relative levels of RL-TERRA
****
D
Control shRNA
METTL3-KD
Control siRNA
RNase H siRNA-1
RNase H siRNA-2
TERRA RNA-FISH
TERRA foci/nucleus
Control-sh + Control siRNA
METTL3-KD + Control siRNA
METTL3-KD + RNase H siRNA-1
METTL3-KD + RNase H siRNA-2
E
RNase HWT
RNase HMut
Merge
S9.6-TRF2 PLA
TRF1-mCherry
PLA foci co-localized with TRF1-mCherry/nucleus
F
Control-sh
METTL3-KD
G
Control siRNA
hnRNPA2B1 siRNA-2

Figure 6

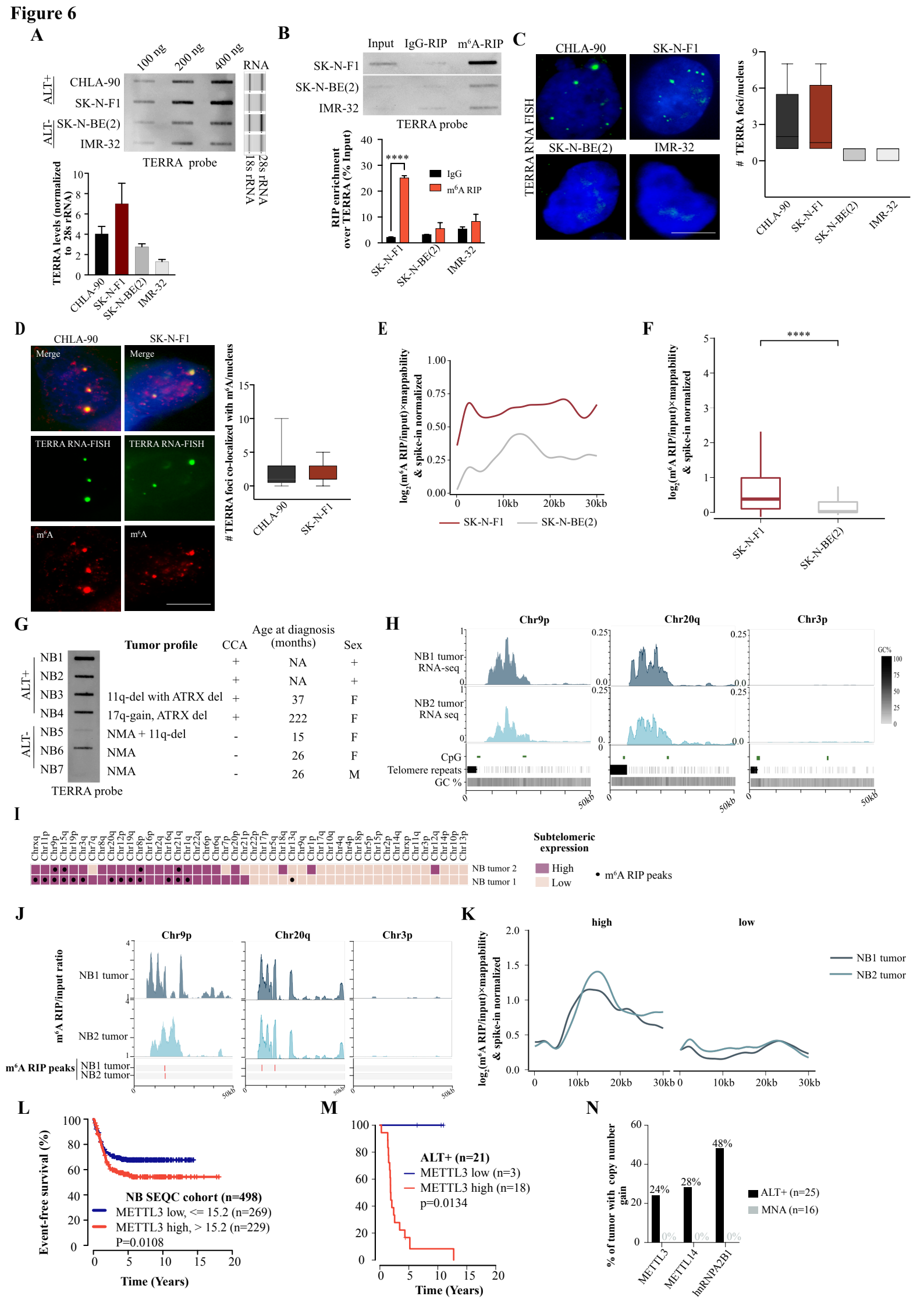
A
100 ng
200 ng
400 ng
RNA
ALT+
CHLA-90
SK-N-F1
ALT-
SK-N-BE(2)
IMR-32
TERRA probe
28s rRNA
18s rRNA
TERRA levels (normalized to 28s rRNA)
B
Input
IgG-RIP
m6A-RIP
SK-N-F1
SK-N-BE(2)
IMR-32
TERRA probe
RIP enrichment over TERRA (% Input)
****
IgG
m6A RIP
C
CHLA-90
SK-N-F1
SK-N-BE(2)
IMR-32
TERRA RNA FISH
TERRA foci/nucleus
D
CHLA-90
SK-N-F1
Merge
TERRA RNA-FISH
m6A
TERRA foci co-localized with m6A/nucleus
E
log2(m6A RIP/input)×mappability & spike-in normalized
10kb
20kb
30kb
SK-N-F1
SK-N-BE(2)
F
****
log2(m6A RIP/input)×mappability & spike-in normalized
SK-N-F1
SK-N-BE(2)
G
Tumor profile
CCA
Age at diagnosis (months)
Sex
NB1 + NA +
NB2 + NA +
NB3 11q-del with ATRX del + 37 F
NB4 17q-gain, ATRX del + 222 F
NB5 NMA + 11q-del - 15 F
NB6 NMA - 26 F
NB7 NMA - 26 M
ALT+
ALT-
TERRA probe
H
Chr9p
Chr20q
Chr3p
NB1 tumor RNA-seq
NB2 tumor RNA seq
CpG
Telomere repeats
GC %
GC%
50kb
I
Subtelomeric expression
NB tumor 2
NB tumor 1
High
Low
m6A RIP peaks
J
Chr9p
Chr20q
Chr3p
m6A RIP/input ratio
NB1 tumor
NB2 tumor
m6A RIP peaks
K
high
low
log2(m6A RIP/input)×mappability & spike-in normalized
NB1 tumor
NB2 tumor
L
Event-free survival (%)
NB SEQC cohort (n=498)
METTL3 low, <= 15.2 (n=269)
METTL3 high, > 15.2 (n=229)
P=0.0108
Time (Years)
M
ALT+ (n=21)
METTL3 low (n=3)
METTL3 high (n=18)
p=0.0134
Time (Years)
N
% of tumor with copy number gain
24%
28%
48%
0%
0%
0%
METTL3
METTL14
hnRNPA2B1
ALT+ (n=25)
MNA (n=16)

Figure 7

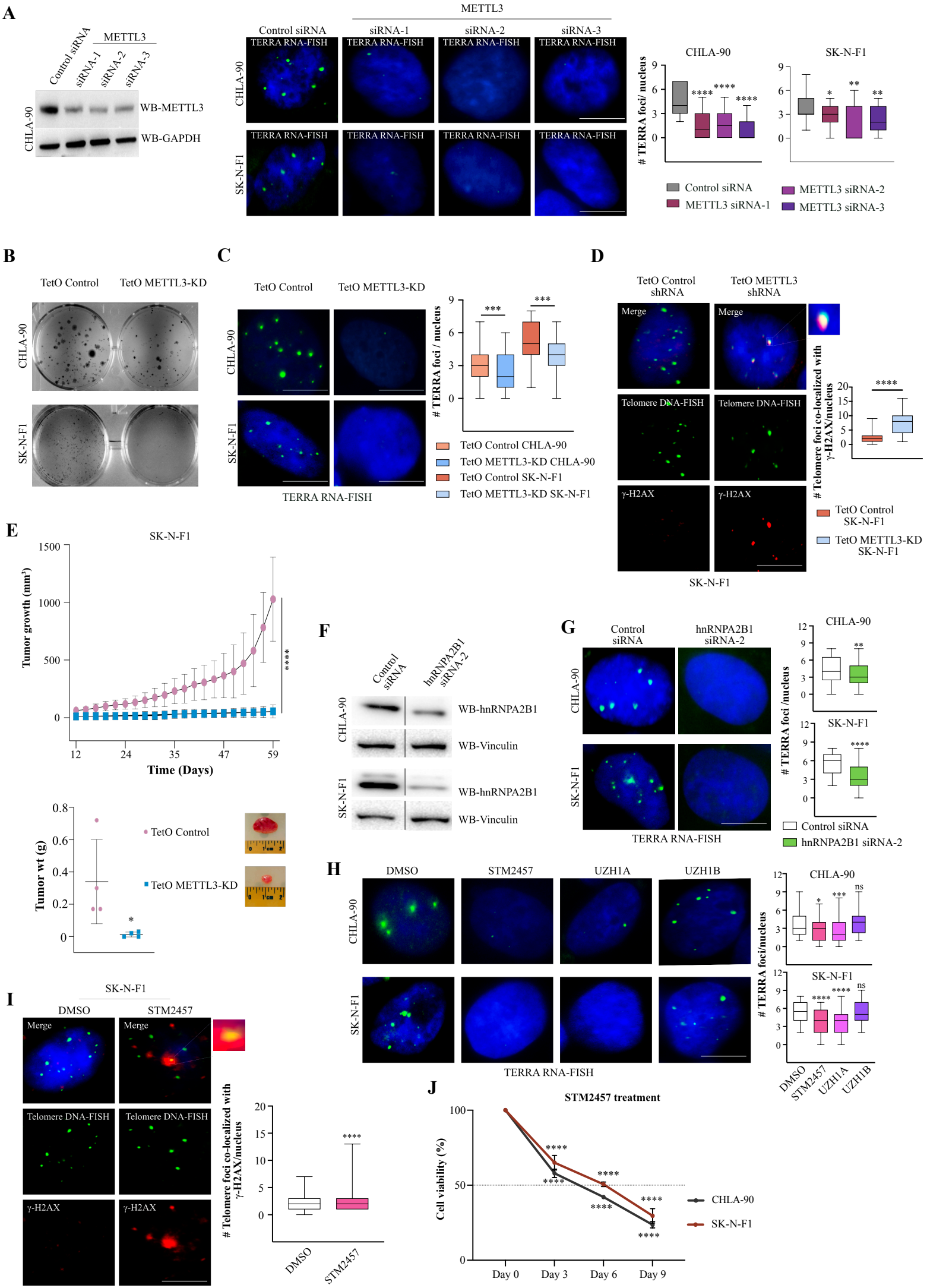
A
METTL3
Control siRNA
siRNA-1
siRNA-2
siRNA-3
CHLA-90
WB-METTL3
WB-GAPDH
TERRA RNA-FISH
SK-N-F1
TERRA foci/ nucleus
Control siRNA
METTL3 siRNA-1
METTL3 siRNA-2
METTL3 siRNA-3
B
TetO Control
TetO METTL3-KD
C
TERRA foci / nucleus
TetO Control CHLA-90
TetO METTL3-KD CHLA-90
TetO Control SK-N-F1
TetO METTL3-KD SK-N-F1
D
TetO Control shRNA
TetO METTL3 shRNA
Merge
Telomere DNA-FISH
γ-H2AX
Telomere foci co-localized with γ-H2AX/nucleus
E
Tumor growth (mm³)
Time (Days)
Tumor wt (g)
F
hnRNPA2B1 siRNA-2
WB-hnRNPA2B1
WB-Vinculin
G
TERRA foci /nucleus
H
DMSO
STM2457
UZH1A
UZH1B
I
J
STM2457 treatment
Cell viability (%)
Day 0
Day 3
Day 6
Day 9